Article

Optimal Water Addition in Emulsion Diesel Fuel Using Machine Learning and Sea-Horse Optimizer to Minimize Exhaust Pollutants from Diesel Engine

Hussein Alahmer [1,*], Ali Alahmer [2,3,*], Malik I. Alamayreh [4], Mohammad Alrbai [5], Raed Al-Rbaihat [3], Ahmed Al-Manea [6] and Razan Alkhazaleh [2]

[1]   Department of Automated Systems, Faculty of Artificial Intelligence, Al-Balqa Applied University, Al-Salt 19117, Jordan
[2]   Department of Industrial and Systems Engineering, Auburn University, Auburn, AL 36849, USA
[3]   Department of Mechanical Engineering, Faculty of Engineering, Tafila Technical University, Tafila 66110, Jordan
[4]   Department of Alternative Energy Technology, Faulty of Engineering and Technology, Al-Zaytoonah University, Amman 11733, Jordan
[5]   Department of Mechanical Engineering, School of Engineering, University of Jordan, Amman 11942, Jordan
[6]   Al-Samawah Technical Institute, Al-Furat Al-Awsat Technical University, Al-Samawah 66001, Iraq
[*]   Correspondence: dr.halahmer@bau.edu.jo (H.A.); aza0300@auburn.edu (A.A.)

Abstract: Water-in-diesel (W/D) emulsion fuel is a potentially viable diesel fuel that can simultaneously enhance engine performance and reduce exhaust emissions in a current diesel engine without requiring engine modifications or incurring additional costs. In a consistent manner, the current study examines the impact of adding water, in the range of 5–30% wt. (5% increment) and 2% surfactant of polysorbate 20, on the performance in terms of brake torque (BT) and exhaust emissions of a four-cylinder four-stroke diesel engine. The relationship between independent factors, including water addition and engine speed, and dependent factors, including different exhaust released emissions and BT, was initially generated using machine learning support vector regression (SVR). Subsequently, a robust and modern optimization of the sea-horse optimizer (SHO) was run through the SVR model to find the optimal water addition and engine speed for improving the BT and lowering exhaust emissions. Furthermore, the SVR model was compared to the artificial neural network (ANN) model in terms of R-squared and mean square error (MSE). According to the experimental results, the BT was boosted by 3.34% compared to pure diesel at 5% water addition. The highest reduction in carbon monoxide (CO) and unburned hydrocarbon (UHC) was 9.57% and 15.63%, respectively, at 15% of water addition compared to diesel fuel. The nitrogen oxides (NOx) emissions from emulsified fuel were significantly lower than those from pure diesel, with a maximum decrease of 67.14% at 30% water addition. The suggested SVR-SHO model demonstrated superior prediction reliability, with a significant R-Squared of more than 0.98 and a low MSE of less than 0.003. The SHO revealed that adding 15% water to the W/D emulsion fuel at an engine speed of 1848 rpm yielded the optimum BT, CO, UHC, and NOx values of 49.5 N.m, 0.5%, 57 ppm, and 369 ppm, respectively. Finally, these outcomes have important implications for the potential of the SVR-SHO approach to minimize engine exhaust emissions while maximizing engine performance.

Keywords: water/diesel emulsion; optimization; machine learning; diesel engine; regression; exhaust emission; engine performance

1. Introduction

Addressing global warming and climate change requires improved engine fuel combustion and the minimization of exhaust emissions. Fuel additives effectively improve fuel characteristics and reduce exhaust engine emissions [1–6]. The addition of water to diesel

fuel has received much attention among the numerous fuel additives studied because of its extraordinary effects on lowering nitrogen oxides (NOx) emissions. The principal mechanism underlying the reduction in NOx emission appears to be a drop in the adiabatic flame temperature due to liquid water evaporation and subsequent dilution of the gas phase species. It is well known that water can reduce the temperature of the cylinder chamber by absorbing the latent vaporization heat [7,8]. Furthermore, the increased specific heat of water lowered the cylinder temperature. A longer ignition delay caused by the addition of water enables better mixing and lowers the soot production rate [9]. Another important combustion property of water-in-diesel (W/D) emulsion fuel is its micro-explosion behavior, which results in smaller fuel droplets after secondary atomization and better combustion efficiency. There are many methods for introducing water into the combustion chamber [10]: (a) injection of liquid or vapor water into the intake air, (b) simultaneous water and diesel injections, and (c) W/D emulsion fuel with or without surfactants. The first two water injection techniques incur extra costs for the water injection system and engine corrosion concerns [11]. However, the third approach has been recognized as the most effective strategy with no additional cost and engine modification required for NOx reduction [12].

1.1. Literature Review on Emulsion Diesel Fuel

Several experiments have been conducted to explore the behavior of diesel engines driven by emulsified fuels. Yang et al. [13] observed that adding 15% water to diesel fuel reduced NOx emissions by 30% at full load at 3200 rpm engine speed, with insignificant increases in brake-specific fuel consumption (BSFC). In contrast to the previous experiments, Liang et al. [14] reported that using a W/D containing 30% water boosted BSFC by 12%. Sudrajad et al. [15] tested a compression ignition (CI) engine operating at a constant speed with various engine loads and fueled by an emulsion fuel comprising 10% water, 1% surfactant, and 89% diesel fuel. Compared to pure diesel fuel, the results showed a reduction in engine emissions such as NOx, carbon monoxide (CO), and sulfur dioxide (SO_2). Mazlan et al. [16] investigated the effects of different water addition amounts (5%, 6.5%, 10.8%, and 30%) on the CI engine performance and exhaust emissions of non-surfactant W/D emulsion fuel. The authors demonstrated that the emulsion fuel with a water content of 6.5% exhibited the lowest fuel consumption and the highest average NOx reduction. Gonguntla et al. [17] operated a single-cylinder CI engine using a W/D emulsion fuel comprising 6% water content. The findings revealed a 24% decrease in NOx and a 42% decrease in CO emissions compared to pure diesel. Furthermore, employing W/D emulsion fuel increased the BSFC by 6.6%. Elsanusi et al. [18] investigated the performance and emissions of a diesel engine using water (5–15% vol.) and biodiesel (0–40%). They observed that W/D with 15% water and 20% biodiesel had the maximum brake thermal efficiency (BTE) under a full load. Furthermore, increasing the water content of the W/D emulsion fuels dramatically decreased NOx emissions. Ali et al. [19] examined the impact of W/D emulsion fuels on CI engine performance and exhaust emissions, concluding that the water content in W/D emulsion fuels containing 10% or less water could be deemed optimal and that W/D emulsion fuel decreased NOx and particulate matter (PM) emissions. Ithnin et al. [20] evaluated four kinds of W/D emulsion fuels, including water in concentrations ranging from 5% to 20% by volume and pure diesel fuel as a baseline. The results revealed that all the W/D blends reduced NOx and PM compared to pure diesel. However, the CO and carbon dioxide (CO_2) emissions increased at low and high loads compared to pure diesel fuel. Yang et al. [21] powered the CI engine using emulsified gasoline with organic additives. They observed that NOx decreased by 30.6%, but CO and HC increased insignificantly. Nour et al. [22] introduced water into the exhaust manifold and opened the exhaust valve during the suction stroke, allowing hot exhaust gases to evaporate water and minimize NOx and soot. They reduced NOx by 85% and soot by 40% while increasing the in-cylinder pressure by 11% compared to exhaust gas recirculation (EGR) without water injection. Choi and Lee [23] found that a W/D comprising 16%

water addition resulted in a lower combustion temperature and decreased NOx and black carbon rates by approximately 60% and 15%, respectively. Attia et al. [24] reported that emulsions containing large water droplets (5.5 μm) reduced NOx emissions by 25%. In comparison, adding tiny water droplets (0.53 μm) to the emulsion reduces smoke and unburned hydrocarbon (UHC) by 80% and 35%, respectively. Lin et al. [25] found that applying W/D emulsion fuel increased CO while decreasing NOx emissions.

1.2. Literature Review on Optimization Methods for Diesel Engine Behavior

Experiments have been conducted to determine the influence of W/D emulsion under various operating situations and to achieve the maximum engine performance while emitting the lowest exhaust pollutants. Since these experimental studies are expensive, restricted in scope, and time-consuming, more efficient procedures are required. Using optimization methods to reduce the requirement for extensive experimental testing is a useful approach [26]. Many researchers have developed and used a wide range of meta-heuristic algorithm optimization methodologies in design analysis, such as genetic algorithm optimization, particle swarm optimization (PSO), whale optimization algorithm (WOA), response surface methodology (RSM), artificial neural network (ANN), Taguchi optimization, grey wolf optimization (GWO), and intelligent grey wolf optimization (IGWO) [27–31]. According to Hoseini and Sobati [32], the optimal formulation for the W/D emulsion diesel fuel was 5% water and 2% surfactant after applying multi-objective optimization. The optimal W/D emulsion fuel significantly reduced NOx (−18.24%) compared to regular diesel fuel. Vellaiyan et al. [33] analyzed a single-cylinder diesel CI engine using W/D fuels with varying water content using the Taguchi technique and L16 orthogonal array design. The results demonstrated that proper parametric settings substantially enhanced combustion, engine performance, and exhaust emissions. Furthermore, Vellaiyan et al. [34] developed a multi-purpose optimization technique for water–biodiesel emulsion fuel with nano additives. The findings showed that the quantity of water in the emulsion exhibited the most significant influence on the performance and exhaust emissions of the CI engine. Khathri et al. [35] employed the RSM technique to improve the performance and minimize the exhaust pollutants of a CI engine driven by W/D emulsion fuel with water contents of 5% and 10% by volume. The results revealed that the optimal engine operating settings were 5% water content, 50% load, and an engine speed of 2446 rpm, while the optimum performance and emissions parameters were brake torque (BT) of 103.7 N.m., brake power (BP) of 26.3 kW, brake thermal efficiency of 43.8%, NOx of 521.8 ppm, and CO of 3.1%. Kumar et al. [36] utilized the ANN-PSO approach to determine the best parameters for producing W/D emulsion fuels for diesel engines. The estimated optimized settings were a W/D emulsion fuel with 20% water, 0.9% surfactant, and 2200 rpm of stirrer for separation processes of 14.33% in one day, with a range of 6.54%.

1.3. Research Gap, Objectives, and Novelty

Although there are numerous articles on the performance, combustion, and emission characteristics of emulsion diesel fuels, there are few studies on the optimal addition of water to minimize exhaust emissions while improving engine performance. Therefore, identifying the optimum potential combination that enhances engine performance necessitates performing trials for all test setups, and mixtures at different amounts are tedious and costly. Instead, the previous concerns can be solved using various optimization techniques, enabling the optimal blending percentage to be selected, leading to the highest engine performance and lowest exhaust emissions. There are no published studies on the use of nonlinear regression with the sea-horse optimizer (SHO) to reduce CI engine exhaust emissions and improve performance. This study introduces a prediction framework based on machine learning support vector regression (SVR) and an innovative swarm intelligence-based metaheuristic, termed the sea-horse optimizer (SHO), which is inspired by the natural mobility, predation, and breeding activities of sea horses. A supervised machine learning model and a learning technique that analyzes data for regression analysis

(SVR) were used in the proposed framework to evaluate the link between the independent factors, including engine speed and water addition%, and the dependent variables, including engine performance in terms of BT and exhaust emissions, which included NOx, UHC, and CO. Subsequently, the SHO technique was utilized to optimize the output of the prediction model by updating the population's current locations in the discrete searching space, obtaining the best engine speed and water addition% for the maximum BT and the least amount of NOx, UHC, and CO. According to the best of the authors' knowledge, no studies have used the most recent optimization approaches, such as SHO, for assessing, optimizing, and enhancing the performance of CI engines driven by W/D emulsion blends with various water additions. Additionally, the present investigation organized and conducted its virtual experiments using the design of experiments (DOE). Accuracy evaluation is a vital part of any machine learning model. The mean squared error (MSE) and coefficient of determination (R^2) were used to evaluate the model's effectiveness in the regression analysis. The expected and realized experimental outcomes are then compared. Furthermore, the SVR model was compared to the artificial neural network (ANN) model in terms of R-squared and MSE. Finally, the optimization of engine exhaust emissions and performance was achieved by comparing the performance of SHO with other meta-heuristic optimization techniques using the Whale Optimization Algorithm (WOA) as a reference. It is worth noting that the SHO approach has effectively handled a variety of difficulties, including numerical challenges with numerous modes and dimensions. The SHO method has many benefits over other meta-heuristic techniques, including ease of use, flexibility, stability, fewer parameters, and improved algorithm performance. Therefore, SHO can replace various standard metaheuristics, such as GWO, PSO, WOA, and other optimizer methods. This is because of its large optimization capacity and low computing cost. This happens because, in early iterations, sea horses tend to use the Brownian motion of floating action and offspring renewal to find the best answer across the entire search space. In later iterations, sea horses used spiral motion and a successful predation stage to find the best response.

2. Engine Test, Experimental Methods, Modeling, and Optimization

A single-cylinder water-cooled CI engine was used to assess the engine performance and exhaust emission behavior when fueled by W/D emulsion fuels. Table 1 lists the technical specifications of the diesel engine used. The emulsion was prepared using a 1500-rpm blender. W/D emulsion combinations with 5–30% volumetric water percentages were prepared. To stabilize the W/D emulsions, a surfactant of Tween 20 was used at 2% volume. The process for creating W/D emulsion fuels involves two stages using a homogenizer emulsification device. In the first stage, Tween 20 surfactant is mixed with diesel fuel. Subsequently, a set amount of water was slowly added to the mixture, while it was agitated at 800 rpm for 5 min, resulting in the formation of pre-emulsions. In the second stage, these pre-emulsions were mixed at a high speed of 5000 rpm for 20 min [37]. The most stable fuel was found to be the 5% W/D emulsion fuel, and all emulsion fuel blends were found to be stable for at least 20 days without any separation. The W/D emulsion's fuel density, viscosity, and calorific value were measured, as displayed in Table 2. For assessing all the W/D emulsion fuel mixes, pure diesel was used as a baseline.

Table 1. Diesel engine specifications.

Parameter	Diesel Engine Specifications
Engine description	Automotive 30 test bed, 4-cylinders, 4-strokes, Direct injection, Naturally aspirated, Water cooled
Bore × Stroke	72.25 × 88.18 mm
Swept volume	1450 cc
Compression ratio	21.5:1

Table 2. Properties of different blends of W/D emulsion fuels.

Properties	Pure Diesel	Water Addition						Test Method	Equipment	Accuracy	Error
		5%	**10%**	**15%**	**20%**	**25%**	**30%**				
Calorific Value (MJ/kg)	43.2	42.56	41.76	38.92	37.6	33.86	31.77	ASTM D240	Automatic adiabatic bomb calorimeter	± 0.04 MJ/kg	$\pm 0.1\%$
Density @ 15 °C (kg/m^3)	0.838	0.851	0.855	0.858	0.862	0.868	0.879	IP 190/93	Capillary stoppered pycnometer	$\pm 10^{-3}$ g/cm^3	$\pm 0.12\%$
Viscosity at 20 °C (Centi-Poise)	4	8	17	43	38	21	18	ASTM D445	EMILA rotary viscometer apparatus	± 0.1 cP	$\pm 2.6\%$

2.1. Engine Performance Measurements

The experiment used a diesel engine connected to a 400 V DC compound wound dynamometer that only absorbed power. The engine was able to reach a maximum speed of 3000 rpm; however, with the use of a belt reduction drive, it could reach 5000 rpm. The belt drive was chosen because it has low friction and hysteresis losses, and it does not require a flexible connection to handle shaft misalignment. The torque measurement accuracy was ± 0.1 N.m, and the rotational speed accuracy was ± 1 rev./min. All engine parameters were evaluated at full load and various speeds. The test procedure for the CI engine was as follows: The engine was warmed up with pure diesel for approximately 10 min until it reached steady-state conditions, and the lubricating oil temperature was maintained between 80 and 90 °C. The throttle was set to wide-open throttle (WOT), and a braking load was applied. Once these conditions were reached, the engine was brought to the required test condition and allowed to run for at least two minutes before collecting data. This time frame was designed to ensure consistent and repeatable operating conditions for the engine, and to provide sufficient time for the engine to stabilize and reach a steady state before collecting data. Then, readings of brake torque, temperatures, rotational speed, fuel weight, and intake volume flow rate were collected and recorded. This procedure was repeated for different W/D emulsion fuels. Before testing, the CI engine and dynamometer were calibrated and set to their default settings. Once the engine stabilized, all data were recorded. Each fuel was tested three times, and the data were averaged. The average time period allowed after experimental recording for an emulsion diesel test was approximately 5 to 10 min. This time frame has been determined to be sufficient to allow the engine to return to normal operating conditions and to enable the engine to cool down, thereby ensuring accurate and reliable results.

It is worth mentioning that the fuel system was designed to provide a consistent and reliable flow of fuel to the engine in accordance with its operating conditions. The fuel delivery system is typically comprised of a fuel tank, a fuel pump, fuel injectors, and a control system to regulate the flow of fuel to the engine. The fuel tank was mounted on top of the overhead frame and has a capacity of 30 L. Fuel measurements were taken using a calibrated pipette gauge with two bulbs. The fuel delivery system was monitored and regulated based on factors such as engine speed, load, and temperature to ensure optimal performance.

2.2. Exhaust Emission Measurement

The exhaust emissions were measured using a Kane automotive gas analyzer. The emissions were tested by attaching a gas probe to the exhaust pipe and then analyzing the exhaust emissions. It is worth noting that the backpressure was avoided by installing an exhaust duct with a diameter of 40 to 50 mm to discharge exhaust gases [38]. The gas analyzer was turned on, and the emission sensors were filled with fresh air. The oxygen sensor was programmed to be 20.9%. During air flow filtering, the time runs down to zero, and the analyzer performs a self-calibration operation. Following the self-calibration, a leak test was performed by attaching a probing seal. The probing seal was eliminated immediately after the leakage test, and the gas analyzer reported zero for CO and CO_2

and set O_2 at 20.9%. The exhaust emission data were collected after the engine achieved working temperature. Each test was performed three times, and the average of the recorded results was calculated. Table 3 lists the specifications and accuracies of the gas analyzer equipment.

Table 3. Gas analyzer technical specification.

Emission	Test Method	Accuracy	Resolution	Maximum Limit
CO_2	ND-IR *	$\pm$5% of reading	0.01%	16%
CO	ND-IR	$\pm$5% of reading	0.01%	10%
UHC	ND-IR	$\pm$5% of reading	1 ppm	5000
NOx	FC **	0–4000 ppm $\pm$4%;	1 ppm	5000

* ND-IR: Nondispersive infrared; ** FC: Fuel cell.

The exhaust emission uncertainty% was calculated using the following formula [29,39]:

$$\% \text{ of uncertainty} = \pm \sqrt{\begin{aligned} &\left\{ (\text{uncertainty of HC})^2 + (\text{uncertainty of O}_2)^2 + (\text{uncertainty of CO}_2)^2 \right. \\ &\left. + (\text{uncertainty of CO})^2 + (\text{uncertainty of NO}_x)^2 \right\} \end{aligned}} \tag{1}$$

The overall uncertainty of the exhaust gases in Equation (1) was 1.1%, indicating that the analyzed data were reliable.

2.3. Modeling: Support Vector Regression (SVR)

The support vector machine (SVM) approach, initially proposed by Vapnik [40], has been widely acknowledged as a significant and practical method for regression and classification. Support vector regression (SVR) is a subset of SVM that addresses regression issues and function estimation. SVR has been employed in many different industries and has experienced significant progress because of its benefits of straightforward structure and simple implementation. Compared to other AI methods, the computational complexity of SVR is determined by the number of support vectors rather than the dimensions of the input data, which avoids the "dimension curse" and reduces the computational cost. Furthermore, SVR is more resistant to noisy data than other advanced machine learning algorithms, such as an artificial neural network (ANN). Therefore, it can effectively use targets with small and medium sample sizes. Moreover, the kind and number of parameters are critical challenges with artificial intelligent (AI) algorithms. For SVR, the kernel function is a parameter that affects accuracy, while for ANN, the most important parameters are the number of layers, their size, the number of training epochs, and the learning rate. In addition, the initial randomization of a network's weight matrix impacts its performance. This is because the accuracy of the neural networks never exceeds a certain threshold if the initial randomization places them close to a local optimization function minimum. However, SVRs are more reliable, and continuously ensure convergence to the global minimum. SVR is a superior option for this task when all of the aforementioned parameters are considered, as well as our training data.

For a non-linear task, the kernel function is used to convert a nonlinear problem with low dimensions into a linear problem with high dimensions, as expressed in Equation (2).

$$f(x) = \omega \varphi(x) + b \tag{2}$$

where *f(x)* is a mapping function (dependent variable), x represents an n-dimensional input (independent variable), ω and b are the weight and constant coefficients, respectively, and

$\varphi(x)$ denotes the kernel function in the feature space. By minimizing the regularized risk function, the coefficients ω *and* b can be estimated by Equation (3):

$$\min \frac{1}{2}\|\omega\|^2 + \frac{c}{n}\sum_{i=1}^{n}\varepsilon(y_i - f(x_i))$$
$$s.t \;\; \varepsilon(y_i - f(x_i)) = \begin{cases} 0 & |y_i - f(x)| \le \varepsilon \\ |y_i - f(x)| - \varepsilon & otherwise \end{cases} \tag{3}$$

where C denotes the penalty factor which aids in balancing the amount of confidence with the empirical risk. The intense loss parameter is represented by ε, and $\varepsilon(y_i - f(x_i))$ stands the insensitive loss function. Consequently, the optimization problem is simplified by the inclusion of two non-negative slack variables, ξ_i *and* ξ_i^*, as presented in Equation (4).

$$min_{\omega,\xi,\xi^*} \; \frac{1}{2}\|\omega\|^2 + C\sum_{i=1}^{n}\left(\xi_i + \xi_i^*\right)$$
$$s.t. \begin{cases} \omega\varphi(x) + b - y_i \le \varepsilon + \xi_i \\ y_i - \omega\varphi(x) - b \le \varepsilon + \xi_i^* \;, \; for \; i = 1,2,\dots,n \\ \xi_i, \xi_i^* \ge 0 \end{cases} \tag{4}$$

The optimization task mentioned in Equation (4) is transformed into a dual optimization problem using Lagrangian multipliers, as illustrated in Equation (5):

$$\min \frac{1}{2}\sum_{i,j=1}^{n}\left(\alpha_i^* - \alpha_i\right)\left(\alpha_j^* - \alpha_j\right)k(x_i.x_j) + \varepsilon\sum_{i=1}^{n}\left(\alpha_i^* + \alpha_i\right) - \sum_{i=1}^{n}y_i\left(\alpha_i^* - \alpha_i\right)$$
$$s.t. \begin{cases} \sum_{i=1}^{l}\left(\alpha_i^* - \alpha_i\right) = 0, \; for \; i = 1,2,\dots,n \\ 0 \le \alpha_i^*, \alpha_i \le C \end{cases} \tag{5}$$

where the kernel function is $k(x_i.x_j)$, and α_i^*, α_i represents the Lagrangian multipliers. In that case, the following Equation (6) was utilized to calculate *f(x)* support vector regression.

$$f(x) = \sum_{i=1}^{n}(\alpha_i - \alpha_i^*)k(x_i, x) + b \tag{6}$$

The kernel function is the most crucial component of the SVR. It transforms a nonlinear problem into a linear problem by projecting the initial low-dimensional data into a higher-dimensional data space [41]. In this study for modeling, the ANOVA radial basis kernel is used because it performs well in multidimensional regression problems [42], as shown in Equation (7). Moreover, the features they employed and how they are weighted are largely controlled by the kernel. In particular, the polynomial kernel can only utilize degree d monomials with a single parameter weighting scheme. The all-subsets kernel can only be used if all of the monomials that map to conceivable subsets of the x input space features are used. However, the set of monomials can be specified with more freedom using the ANOVA radial basis kernel.

$$k(x_i, x_j) = \sum_{k=1}^{n}exp\left(-\sigma\left(x_i^k - x_j^k\right)^2\right)^d \tag{7}$$

where σ is a tuning parameter, and d is a regression degree.

2.4. Paramteric Optimzation: Sea-Horse Optimizer (SHO)

Optimization problems are problems that should identify the best solution to fulfill the constraints and maximize or minimize the objective function. In general, metaheuristic algorithms, a community of nature-inspired approaches with specialized stochastic operators, have been developed to address these difficult challenges [43]. The sea-horse optimizer (SHO) is a revolutionary swarm intelligence-based metaheuristic introduced by

Zhao et al. [44]. It is influenced by the natural movement, predation, and breeding activities of sea horses. The proposed SHO algorithm comprises three key components: mobility, predation, and breeding. In order to balance the exploitation and exploration of SHO, local and global search algorithms have been developed for the social behaviors of mobility and predation, respectively. The breeding activity is carried out once the first two activities are completed, as explained below.

First, in mobility behavior, the tail of the sea horse periodically wraps around an algal stem (or leaf), which is a feature of its movement patterns. The sea horse is moving in a spiral because the algae stems are experiencing spiral floating modifications around the roots owing to the action of marine vortices at this time. Brownian motion is apparent when the sea horse has suspended upside-down from floating algae or other matter and is pushed about randomly by the waves.

Second, while engaged in predatory behavior, sea horses employ the unique shape of their heads to sneak up on their prey and catch it with up to a 90% success rate.

Finally, when it comes to breeding, male and female sea horses marry at random to form a new generation, which helps the children inherit some beneficial features from their parents.

Consequently, these three acts enable sea horses to survive and adapt to their surroundings. The three aforementioned characteristics are the primary motivations for the proposed SHO algorithm.

The SHO is divided into four phases: (A) initialization, (B) mobility behavior, (C) predation behavior, and (D) breeding behavior of sea horses, as detailed in the subsections below.

2.4.1. Initialization Phase

Similar to other metaheuristics, the SHO algorithm starts with population initialization. If each sea horse represents a potential solution to a problem in the search space, then the entire population of sea horses (referred to as seahorses) can be expressed as follows in Equation (8):

$$S = \begin{bmatrix} x_1^1 & \cdots & x_1^D \\ \vdots & \ddots & \vdots \\ x_P^1 & \cdots & x_P^D \end{bmatrix} \tag{8}$$

where s denotes the seahorses, D indicates the variable's dimension, while P signifies the population size.

The lower bound (LB) and upper bound (UB) of a given problem were used as the starting points for the random generation of each solution. In the search space $[LB, UB]$, the Equations (9) and (10) for the ith individual X_i are presented as follows:

$$X_i = \left[x_i^1, \ldots, x_i^D \right] \tag{9}$$

$$x_i^j = rand * \left(UB^j - LB^j \right) + LB^j \tag{10}$$

where $rand$ stands for the random number between [0, 1], x_i^j stands for the jth dimension in the ith individual, i is an integer with a positive value between 1 and P, and j is an integer with a positive value between [1, D]. The optimized lower and upper bounds of the jth variable of the optimized problem are denoted by LB^j and UB^j, respectively.

Using the minimum/maximum optimization task, the best individual is designated by the X_{best} and is thought to have the lowest/highest fitness level. Equation (11) can be used to obtain X_{best}.

$$X_{best} = arg_{\min \ or \ max}(f(X_i)) \tag{11}$$

where $f(X_i)$ represents the value of the objective function for a specific task.

2.4.2. Movement Behavior Phase

The diverse movement patterns of sea horses during movement behavior generally correspond to a normal distributed random distribution (0, 1). To trade off exploration and exploitation performance, we set $r_1 = 0$ as the cut-off point, with half going to local mining and the other to global search. As a result, the two phases that follow can be used to characterize the movement behavior.

Step 1:

The spiral movement of the sea horse is in conjunction with the vortex of the ocean. When the normal random value r_1 is situated on the right side of the cut-off point SHO, this is primarily exploited locally. Sea horses follow the spiral motion in the direction of the best solution X_{best}. In particular, the Lévy flight [3] is utilized to model the sea horse movement step size, which is beneficial for the sea horse, with a high probability of crossing to other spots in early iterations. Furthermore, it prevents the SHO from becoming unduly localized. The spiral motion of the sea horse continually changes the rotation angle in order to increase the neighbors of the current local solutions. In this instance, Equation (12) can be used to generate a new location of a sea horse.

$$X^1_{new}(t+1) = X_i(t) + Levy(\lambda)((X_{best}(t) - X_i(t)) * x * y * z + X_{best}(t))$$
$$s.t \begin{cases} x = p * cos(\theta) \\ y = p * sin(\theta) \\ z = p * \theta \\ p = u * e^{\theta v} \end{cases} \tag{12}$$

where x, y, and z are the three-dimensional coordinates (x, y, and z) under the spiral movement, respectively. These coordinates are useful for updating the positions of the search agents. The length of the stems (p) is denoted by the logarithmic spiral constants u and v, which are set to 0.05 for each u and v, respectively. The value of θ is chosen at random between $[0, 2\pi]$. The Lévy flight distribution function, ($Levy(z)$), is computed using Equation (13).

$$Levy(z) = s * \frac{\omega * \sigma}{|k|^{\frac{1}{\lambda}}} \tag{13}$$

where ω and k is a random positive number between 0 and 1, s is a constant number of 0.01, and λ is a random value between 0 and 2 (in this work, $\lambda = 1.5$), while σ is computed by applying Equation (14).

$$\sigma = \left(\frac{\Gamma(1+\lambda) * sin\left(\frac{\pi\lambda}{2}\right)}{\Gamma\left(\frac{1+\lambda}{2}\right) * \lambda * 2^{\left(\frac{\lambda-1}{2}\right)}} \right) \tag{14}$$

Step 2:

This step illustrates the Brownian motion of the sea horse in reaction to the waves. When r_1 is situated on the left side of the cut-off point, the SHO inquiry is performed while drifting. In this case, the search operation is critical for avoiding SHO at the local extremum. Brownian motion is employed to simulate the extended moving length of the sea horse so that it can explore the search space more efficiently. The mathematical formulation for this scenario is provided by Equation (15).

$$X^1_{new}(t+1) = X_i(t) + rand * l * \beta_t * (X_i(t) - \beta_i * X_{best})$$
$$s.t \left\{ \beta_t = \frac{1}{\sqrt{2\pi}} \exp\left(-\frac{x^2}{2}\right) \right. \tag{15}$$

where l denotes the constant coefficient of 0.05. The Brownian motion random walk coefficient is denoted by β_t.

These two circumstances can be combined in Equation (16) to obtain the new location of the sea horse at iteration t.

$$X_{new}^1(t+1) = \begin{cases} X_i(t) + Levy(\lambda)((X_{best}(t) - X_i(t)) * x * y * z + X_{best}(t)) & , r_1 > 0 \\ X_i(t) + rand * l * \beta_t * (X_i(t) - \beta_i * X_{best}) & , r_1 \le 0 \end{cases} \quad (16)$$

2.4.3. Predation Behavior Phase

When it comes to feeding on zooplankton and tiny crustaceans, the sea horse can achieve either success or failure. Given that the sea horse has a higher than 90% probability of obtaining food, the random number r_2 of SHO is generated to differentiate between these two possibilities and is set to a critical value of 0.1.

The success of the predation highlights SHO's ability to exploit, since the best, to some extent, reveals the general location of the victim. If r_2 was greater than 0.1, the sea horse's predation was successful. It creeps up on the target (the best), outruns the target, and eventually catches it. If the predation fails, both respond with the reverse response speed as before, indicating that the sea horse will likely continue scouring the region. This predation behavior can be mathematically represented by Equation (18):

$$X_{new}^2(t+1) = \begin{cases} \alpha * (X_{best} - rand * X_{new}^1(t)) + (1 - \alpha) * X_{best} & if\ r_2 > 0.1 \\ (1 - \alpha) * (X_{new}^1(t) - rand * X_{best}) + \alpha * X_{new}^1(t) & if\ r_2 \le 0.1 \end{cases} \quad (17)$$

where r_2 is a random integer value between [0, 1], and $X_{new}^1(t)$ is the new position of the sea horse following movement at iteration t. To change the sea horse's moving step size for pursuing prey, it decreases linearly with iterations and is calculated using Equation (18), where T is the maximum number of iterations.

$$\alpha = \left(1 - \frac{t}{T}\right)^{\frac{2t}{T}} \quad (18)$$

2.4.4. Breeding Behavior Phase

The population was divided into male and female groups based on their fitness levels. Since male sea horses breed, the SHO technique employs half of the population with the highest fitness ratings as fathers and the other half as mothers. As indicated in Equation (19), this division prevents the over-localization of new solutions and promotes the inheritance of beneficial features by fathers and mothers for the next generation.

$$\begin{cases} fathers = X_{sort}^2(1 : \frac{p}{2}) \\ mothers = X_{sort}^2(\frac{p}{2} + 1 : p) \end{cases} \quad (19)$$

where all of the X_{new}^2 are indicated by X_{sort}^2, in ascending order of fitness values. The male and female populations are represented by the mothers and fathers, respectively.

Random mating between males and females produces new offspring. In order for the proposed SHO approach to execute swiftly, it is assumed that each pair of sea horses generates only one child, as illustrated in Equation (20).

$$X_i^{offspring} = r_3 X_i^{father} + (1 - r_3) X_i^{mother} \quad (20)$$

where r_3 is an integer number chosen randomly from [0, 1]. A positive value falls between [1, $p/2$] denoted by i. Male and female randomly chosen members are represented by the X_i^{father} and X_i^{mother}, respectively. The SHO pseudo code is presented in Table 4.

Table 4. The SHO pseudo code.

SHO pseudo Algorithm
Initialize population X_i
Evaluate the fitness of each search agent
Assign X_{best} = the best search agent
While (t < T)
If r1 = randn > 0 **Then**
Set u = 0.05, v = 0.05
Rotation angle Rand $(-2\pi, 2\pi)$
Generate Levy coefficient by Equation (13)
Update agent position by Equation (12)
Else
Set P = 0.05
Update agent position by Equation (15)
End if
Update agent position by Equation (17)
Evaluate fitness of each search agent
Select fathers and mothers by Equation (19)
Calculate breed offspring by Equation (20)
Evaluate fitness value of each offspring
Select next iteration population from the offspring and parents (top p in fitness value)
Update X_{best}
Set t = t + 1
End while
Return X_{best}, f_{best}

A schematic illustration of the experimental strategy combined with the optimization method is presented in Figure 1.
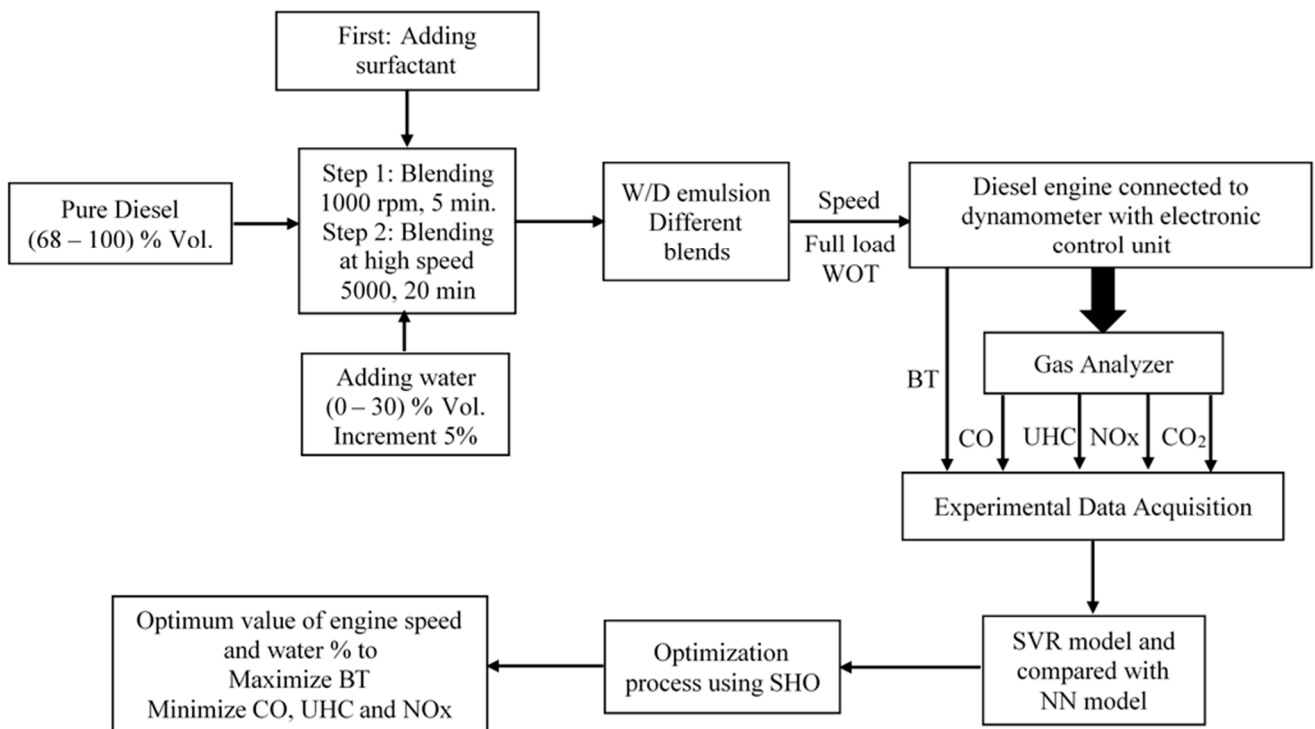

Figure 1. A conceptualization of the experimental approach coupled with an optimization technique.

3. Results and Discussion

3.1. Experimental Analysis

Figure 2 displays the effect of the W/D emulsion fuel on the exhaust gas temperature of a diesel engine at various engine speeds. As indicated, the exhaust temperature dropped as the proportion of water percentage in the W/D emulsion diesel increased. This can be attributed to the heat absorbed by the high water content in the emulsion fuel. Furthermore, the latent heat of water cooled the engine combustion chamber due to the evaporation phenomenon. Therefore, the average temperature of the engine cylinder after the fuel injection and before ignition decreases as the water percentage in the W/D emulsion fuel increases. Alahmer [12] showed that the reduction in exhaust gas temperature is caused by finely distributed water droplets in the W/D emulsion fuel, resulting in a heat sink criterion.
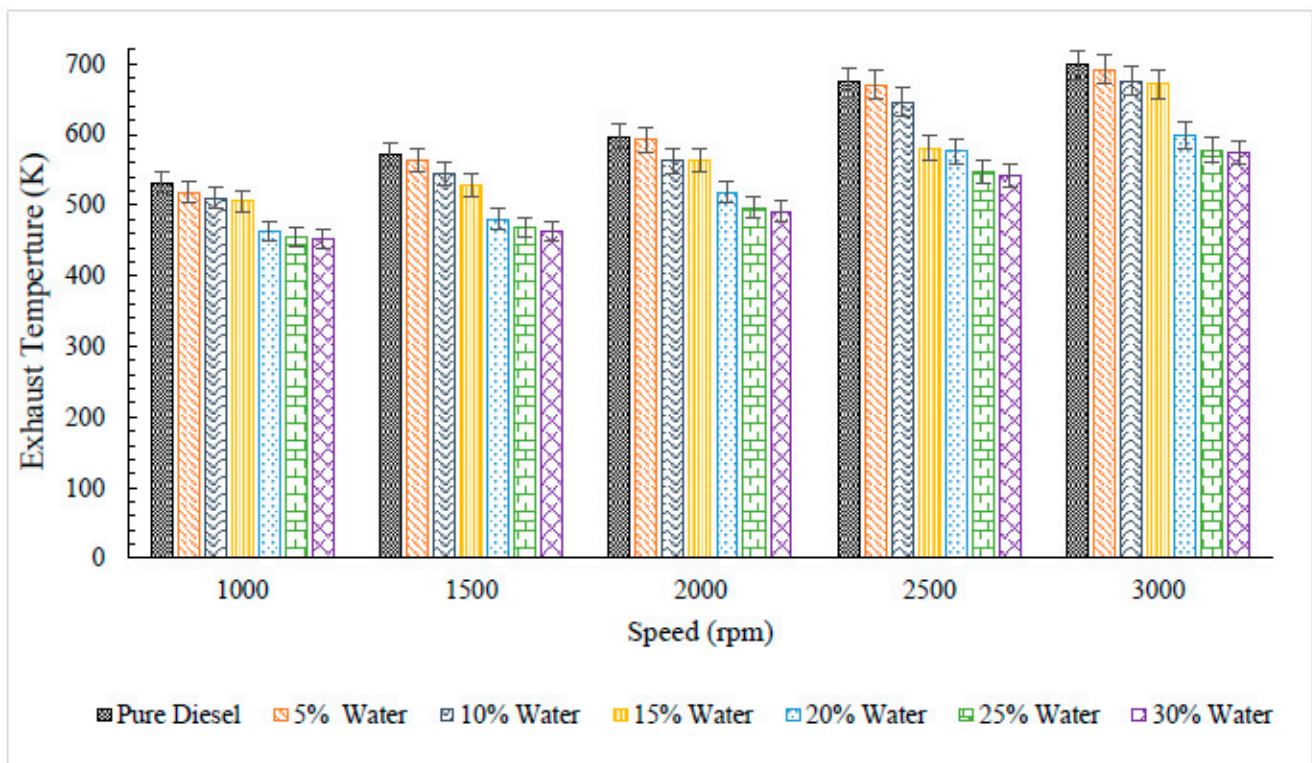
Figure 2. Effect of water-in-diesel emulsion fuel on exhaust gas temperature of a diesel engine at different engine speed.

Figure 3 illustrates the influence of the W/D emulsion fuel on CO_2 exhaust emissions from a diesel engine at different engine speeds. As shown, the amount of CO_2 released increased as engine speed increased. At low water addition amounts of up to 15%, the diesel engine emitted more CO_2 than pure diesel. The excess oxygen atoms in the combustion mixtures were primarily responsible for the increase in CO_2 emissions compared to pure diesel. Consequently, the mixture became lean as the concentration of oxygen atoms in the mixture increased. Furthermore, this may be ascribed to the burning of emulsified fuels causing a significant amount of micro-explosion, resulting in a higher degree of mixing of the reactant mixture. When more than 15% water is added, the diesel engine emits less CO_2 than when a low percentage of water is added. This is because of the high-water content in the W/D emulsion, which significantly reduced the flame temperature. Therefore, the temperature is inadequate for converting CO to CO_2 [45]. Table 5 shows the average fluctuation in CO_2 for varying water additions of the W/D emulsion fuel compared to pure diesel fuel.
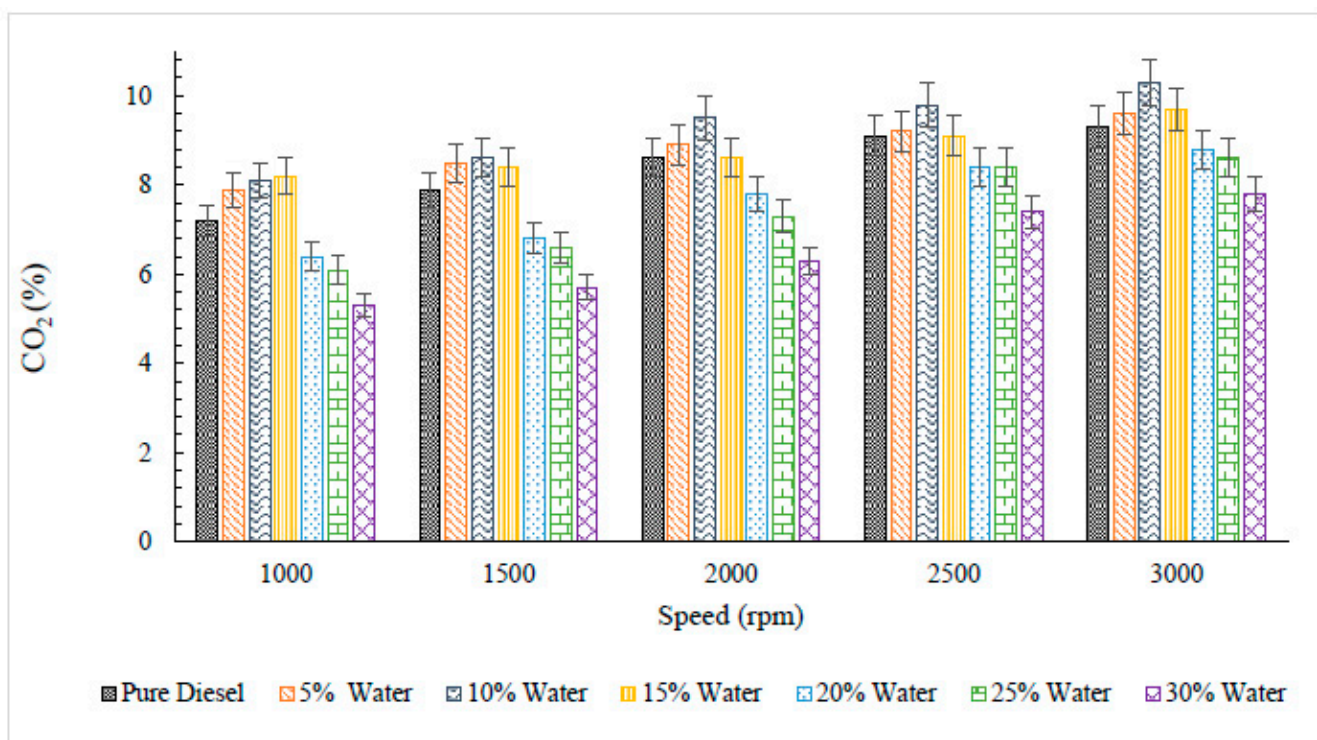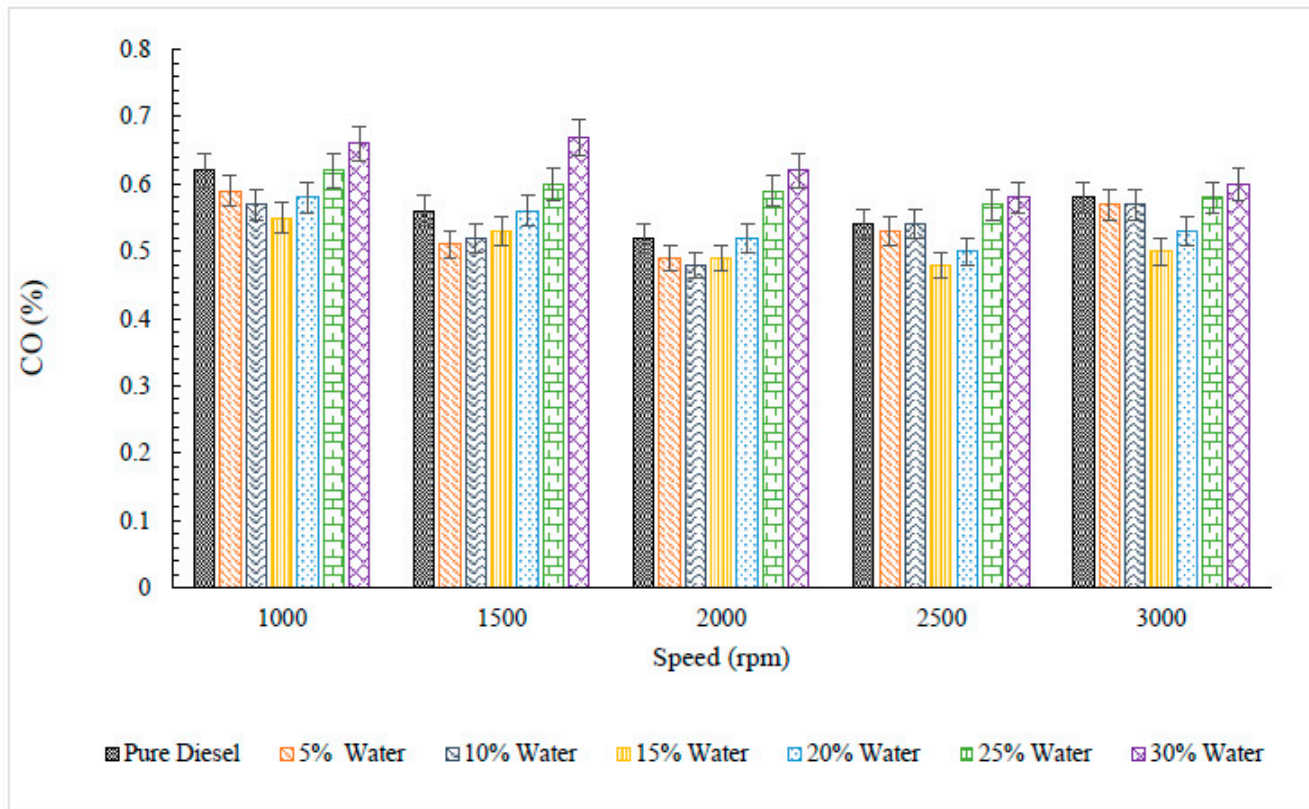
Figure 3. Effect of water-in-diesel emulsion fuel on carbon dioxide emitted from a diesel engine at different engine speed.

Table 5. The average variation in engine performance and exhaust emission for varying water additions of W/D emulsion fuel compared pure diesel fuel.

Water Addition	5%	10%	15%	20%	25%	30%
BT	3.34%	−0.54%	−7.61%	−17.09%	−26.11%	−34.27%
CO_2	4.75%	9.98%	4.51%	−9.26%	−12.11	−22.80%
CO	−4.61%	−4.96%	−9.57%	−4.61%	4.96%	10.99%
UHC	−3.75%	−5.63%	−15.63%	−7.19%	0.63%	16.25%
O_2	11.35%	17.54%	22.36%	38.62%	45.90%	46.93%
NOx	−3.22%	−9.60%	−20.42%	−53.40%	−64.38%	−67.14%

Figure 4 depicts the impact of the W/D emulsion fuel on CO exhaust emissions from a diesel engine at different engine speeds. According to Figure 4, the percentage of CO emitted for all examined emulsion fuels decreased with increasing engine speed until attaining a minimum. Subsequently, the emitted CO emissions increased. This can be attributed to incomplete combustion caused by a lean mixture burning at a low speed. The additional increase could be spurred by ignition timing retardation, which causes more CO to be released at higher engine speeds and the limited time allowed to oxidize all CO atoms [46]. The impact of emulsion fuel on the CO released from a diesel engine is divided into two scenarios: when the diesel engine was run on W/D emulsion fuel with less than 15% water content, the CO emitted reduced as the water content increased. This is referred to as the effect of a micro-explosion process that may result in complete combustion. When using W/D emulsion fuel with more than 15% water content, the CO released increased as the water content increased. The highest increment of CO was 10.99% with 30% water addition, compared to pure diesel. This was due to a significant decrease in the combustion and flame temperatures, which impacted the oxidation of CO. According to Koc and Abdallah [47], the higher CO emissions when water addition increases are due to

the large quantity of radical OH in water, which is accountable for the high levels boosting carbon oxidation to CO. Table 5 displays the average variation in the CO for varying water additions of the W/D emulsion fuel compared pure diesel fuel.

Figure 4. Effect of water-in-diesel emulsion fuel on carbon monoxide emitted from a diesel engine at different engine speed.

Figure 5 shows the variation in the UHC emitted from a diesel engine run by different W/D emulsion fuels at the engine speed. As shown, the amount of UHC emitted from a diesel engine decreases with increasing engine speed. Consequently, a higher speed sustains a more efficient mixture of air and fuel, resulting in improved combustion [29,48]. Another observation is that when the diesel engine run by W/D emulsion diesel fuel contains water less than 15% water addition, the UHC emissions decrease. However, when the diesel engine run by W/D emulsion diesel fuel has more than 15% water, the UHC emissions increase. The highest increment of UHC was 16.25%, with 30% water addition compared to pure diesel. The reduction in UHC emissions is due to the consequence of a micro-explosion process that might result in total combustion. The increase in UHC emissions is due to the impact of increasing ignition delay and decreasing combustion and flame temperature, affecting combustion efficiency [49]. Table 5 demonstrates the average variation in the UHC for varying water additions of the W/D emulsion fuel compared to pure diesel fuel.
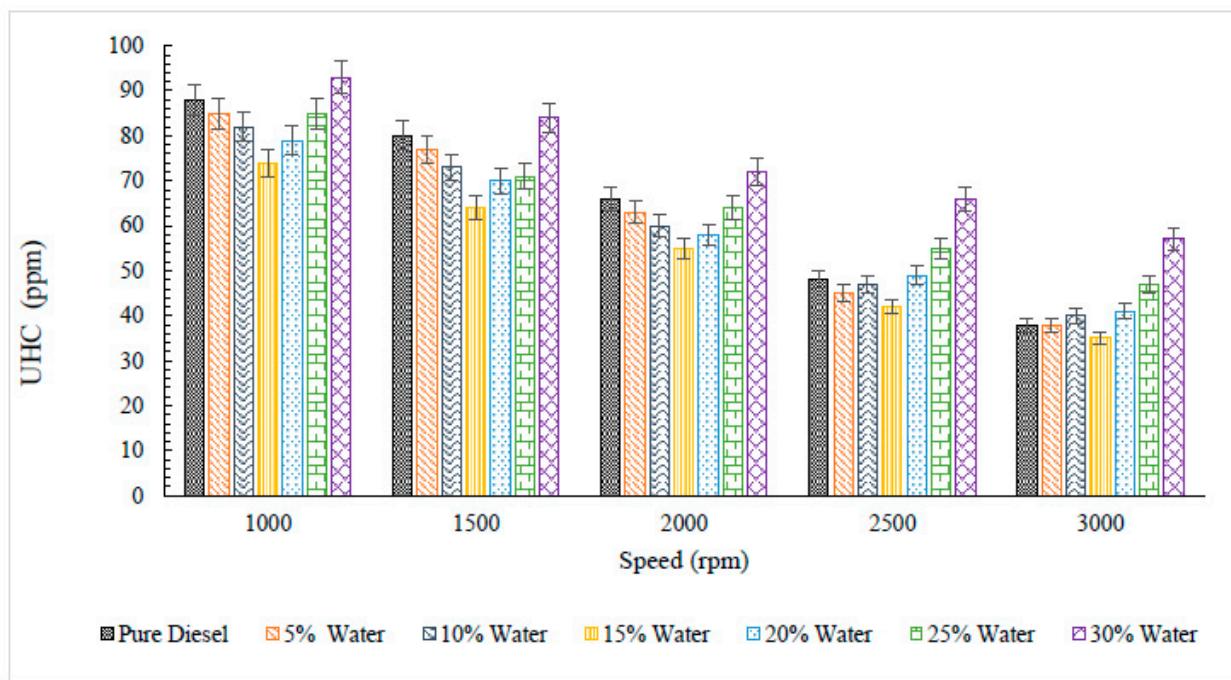
Figure 5. Effect of water-in-diesel emulsion fuel on carbon monoxide emitted from a diesel engine at different engine speed.

Figure 6 depicts the fluctuation in O_2 emissions with engine speed for several W/D emulsions. As the proportion of water in the W/D emulsion increased, the quantity of oxygen released increased. This is owing to the higher amount of oxygen atoms in the W/D emulsion fuel [50]. On average, the highest O_2 released was 46.93% at 30% water addition, compared to pure diesel. Table 5 displays the average variation in O_2 for varying water additions of the W/D emulsion fuel compared to pure diesel fuel.
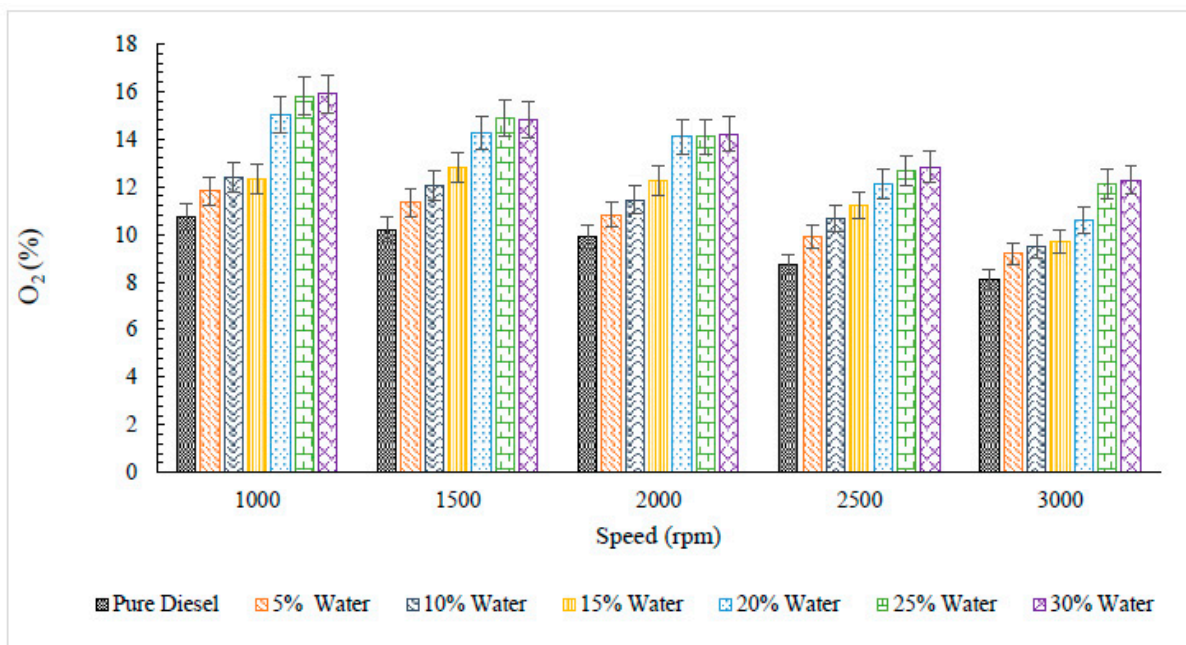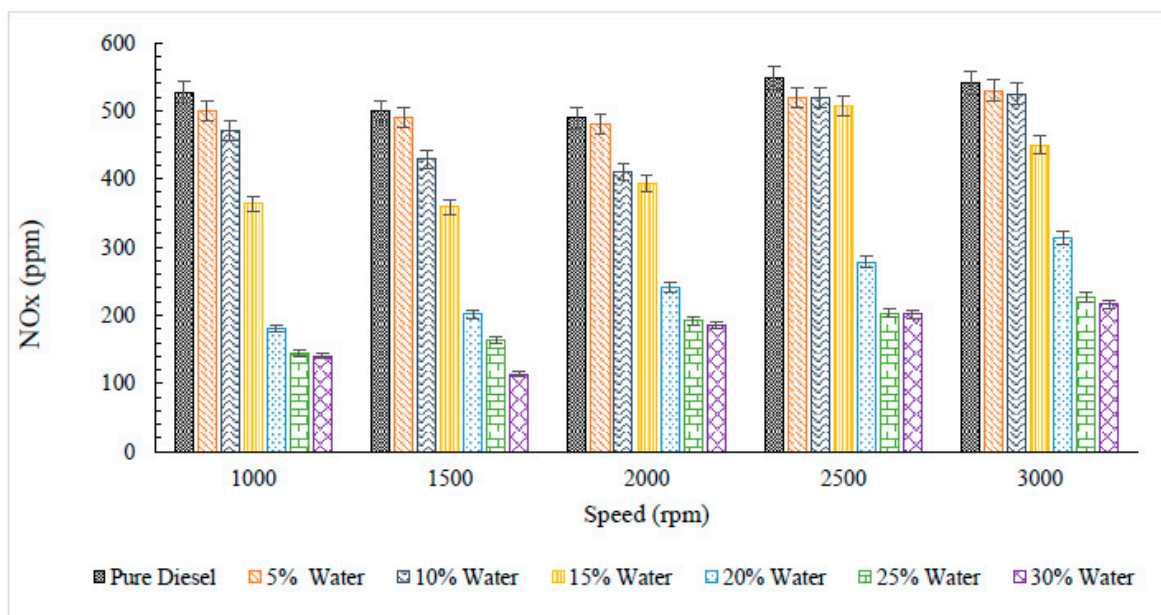

Figure 6. Effect of water-in-diesel emulsion fuel on oxygen dioxide emitted from a diesel engine at different engine speed.

Figure 7 depicts the fluctuation of NOx with engine speed for various emulsions. The engine speed has little influence on NOx generation compared to the amount of water in the W/D emulsion fuel. Compared to pure diesel, the combustion of W/D emulsion fuels generated significantly less NOx. This was attributed to the heat sink phenomenon, which lowed the adiabatic flame temperature. It is well known that NO formation is directly related to high combustion temperature. The temperature was reduced owing to the high latent heat from water evaporation in the W/D emulsion, which absorbed heat during combustion. Jazair et al. [51] stated that the phase change causes a decrease in NOx from water to steam; the endothermic process occurs in the combustion chamber, resulting in a decrease in the in-cylinder temperature. According to Farfaletti et al. [52], the heat sink effect lowers the combustion temperature. The inner water phase of an emulsion fuel partially absorbs the heat generated when the fuel is burned. This can result in a cooler flame and a reduction in the overall heat output of the fuel. Additionally, the water droplets can act as a heat sink, helping to stabilize the combustion process and reduce emissions [53,54]. Consequently, this lowers the temperature of the burning gases during combustion, which limits the production of NOx. According to Dryer [55], the presence of water in the emulsion increases the concentration of hydroxyl (OH) radicals, which in turn leads to a decrease in NOx. However, this explanation contradicts the results reported by Ballester et al. [56]. They investigated the flames of the W/D emulsion blends and pure diesel. The authors assessed the regional distribution of the flame temperature as well as species concentrations of O_2, UHC, CO, and NOx. They observed that the concentration of gases in the inner core of flames during combustion was almost the same for the W/D emulsion fuel and diesel fuel. According to the authors, the decrease in NOx cannot be attributed to changes in gas composition. Moreover, they identified that a decrease in NOx generation occurred as the combustion process was near completion. The peak flame temperature was found in this region, and it was estimated to be reduced by 65 K compared to pure diesel fuel. This study demonstrated that thermal-NO production strongly depends on the peak flame temperature. Table 5 presents the average fluctuation in NOx for varying water additions of the W/D emulsion fuel compared to pure diesel fuel.

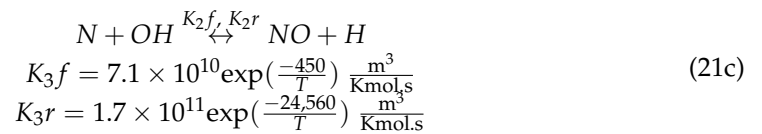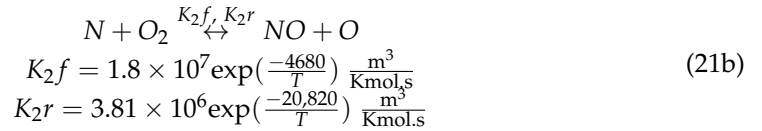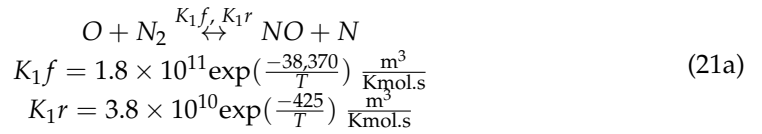**Figure 7.** Effect of water-in-diesel emulsion fuel on nitrogen oxides emitted from a diesel engine at different engine speed.

It is worth noting that the reduction in combustion temperature as a result of increased water content in emulsion has a direct impact on NO formation. This is because the slower chemical reaction rates lead to a decrease in NO production. This relationship can be seen

through the Zeldovich mechanism reactions, where the rate of NO formation is influenced by combustion temperature [57,58].

$$O + N_2 \overset{K_1f, K_1r}{\longleftrightarrow} NO + N$$
$$K_1f = 1.8 \times 10^{11} \exp\left(\frac{-38{,}370}{T}\right) \frac{m^3}{Kmol.s}$$
$$K_1r = 3.8 \times 10^{10} \exp\left(\frac{-425}{T}\right) \frac{m^3}{Kmol.s} \tag{21a}$$

$$N + O_2 \overset{K_2f, K_2r}{\longleftrightarrow} NO + O$$
$$K_2f = 1.8 \times 10^{7} \exp\left(\frac{-4680}{T}\right) \frac{m^3}{Kmol.s}$$
$$K_2r = 3.81 \times 10^{6} \exp\left(\frac{-20{,}820}{T}\right) \frac{m^3}{Kmol.s} \tag{21b}$$

$$N + OH \overset{K_2f, K_2r}{\longleftrightarrow} NO + H$$
$$K_3f = 7.1 \times 10^{10} \exp\left(\frac{-450}{T}\right) \frac{m^3}{Kmol.s}$$
$$K_3r = 1.7 \times 10^{11} \exp\left(\frac{-24{,}560}{T}\right) \frac{m^3}{Kmol.s} \tag{21c}$$

where K_1, K_2, and K_3 are the reaction rate constants in the Arrhenius law. The letters f and *r*, used as subscripts in the reaction constant *k*, indicate the forward and reverse directions of the reaction, respectively.

Figure 8 illustrates the impact of the percentage of water addition in W/D emulsions on the engine bake torque at different speeds. The BT increases with engine speed to an optimum amount, beyond which it begins to drop owing to friction losses and the inability of the engine to consume a complete charge of air at high speeds. When the engine runs on 5% water added to the W/D emulsion fuel at 2000 rpm, the BT generated is at its optimum. This is consistent with Dryer's [21] finding that water in W/D emulsion diesel fuel enhances the combustion mechanism due to simultaneous additional braking of the droplets, which boosts the evaporation surface of droplets and enhances the mixing of the burning fuel in air. The BT decreased as the proportion of water in the W/D emulsion increased. This is due to the increased push on the top of the piston generated by the steam pressure. This process generates tremendous pressure when the charge is ignited in the cylinder. Furthermore, the addition of more than 5% water reduced the heating value of the fuel. Table 5 exhibits the average variation in BT for varying water additions of the W/D emulsion fuel compared to pure diesel fuel.
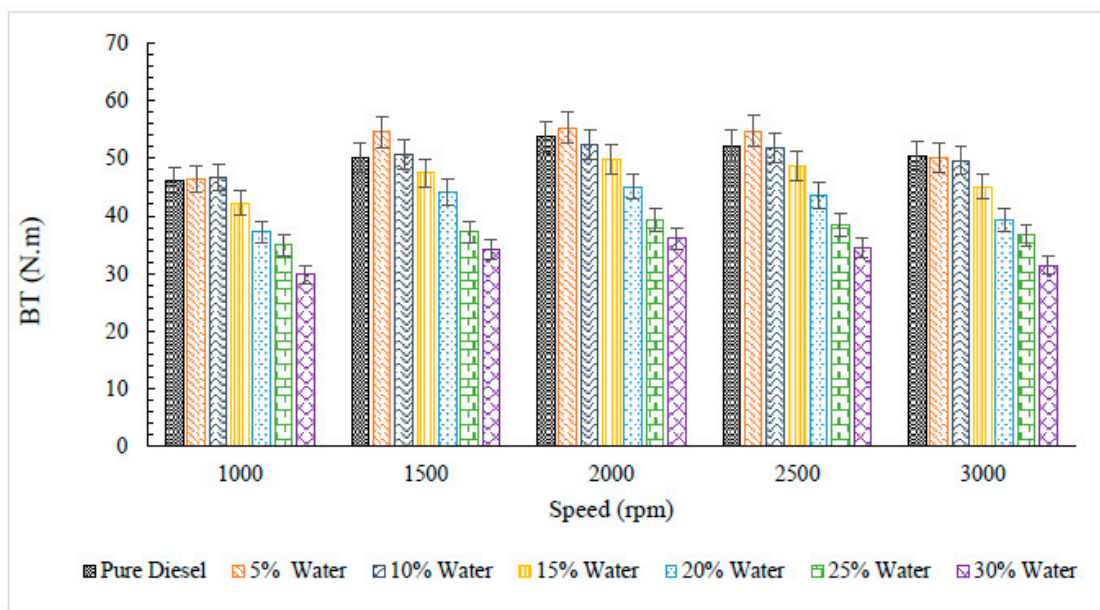

Figure 8. Effect of water-in-diesel emulsion fuel on brake torque of a diesel engine at different engine speed.

It is important to note that previous research has thoroughly examined the effects of various emulsion diesel blends on CI engine performance in terms of brake power (BP), brake thermal efficiency (BTE), and brake specific fuel consumption (BSFC). This study, however, focuses on optimizing the water content while considering the overall behavior of the CI engine, including BP, BTE, and BSFC [59].

3.2. Support Vector Regression Modeling

The experiments were performed using MATLAB R2018a on a Windows 10 64-bit computer with an Intel Core I5-11th generation processor and 8 GB of RAM. The experiment was conducted in two stages. First, regression modeling is based on support vector regression to predict the relationship between variables (engine speed and water addition in the W/D emulsion fuel) and response (BT as an indicator of engine performance and exhaust emissions). Second, SHO optimization was applied to maximize BT and minimize NOx, UHC, and CO emissions. The SVR and ANN parameters for the modeling are presented in Table 6.

Table 6. Parameters of SVR and ANN models.

Experiment	SVR Parameter			ANN Parameter			
	σ	C	d	Hidden Layers	Learning Rate	Epoch	Momentum
BT	1	20.175	3	4	0.1	10	0.05
CO	0.3	0.472	3	4	0.01	10	0.05
UHC	0.5	52.371	2	3	0.1	10	0.05
NOx	1.5	209.802	4	3	0.1	10	0.05

The precision prediction model for engine performance in terms of BT and different exhaust emissions, including CO, UHC, and NOx, was constructed using the SVR technique. The sample data were divided into two parts: N-m data were used to predict the test, and m data were used as training samples to build the predictive model.

The mean square error (MSE) and determination of coefficient (R^2) can serve as indicators of a model's efficacy in regression prediction tasks, as presented in Equations (22) and (23), respectively.

$$\text{MSE} = \frac{1}{n} \sum_{i=1}^{n} (O_i - T_i)^2 \tag{22}$$

$$R^2 = \frac{\left(n \sum_{i=1}^{n} O_i . T_i - \sum_{i=1}^{n} O_i . \sum_{i=1}^{n} T_i\right)^2}{\left(n \sum_{i=1}^{n} O_i^2 - \left(\sum_{i=1}^{n} O_i\right)^2\right) \left(n \sum_{i=1}^{n} T_i^2 - \left(\sum_{i=1}^{n} T_i\right)^2\right)} \tag{23}$$

where n stands for the test set, T stands for the target value, and O stands for the anticipated result of the ith set of data. It is worth noting that the prediction accuracy improved as the MSE decreased. The R^2 value determines the degree of the correlation. The fitting percentage improves as R^2 approaches 1. Table 7 compares the SVR model assessment to the ANN model utilizing the rectified linear unit (ReLU) for the hidden layers to analyze the effectiveness of the proposed model. Table 7 compares the performance of the two models based on MSE and R^2 scores and indicates that the SVR outperforms the ANN, particularly for small datasets, because it is more robust to noisy data. Furthermore, local minima constitute a barrier for ANNs, implying that loss function minimization may fail.

A graphical representation was developed to assess the SVR model. To demonstrate the prediction accuracy of the models, their forecasts were plotted against the respective targets for each experiment (BT, CO, UHC, and NOx), as shown in Figure 9. This shows how well the SVR models mimic the provided observations.

Table 7. Statistical comparison of the SVR prediction model to the ANN model.

Experiment	SVR Model		ANN Model	
	MSE	R^2	MSE	R^2
BT	0.00309	0.9883	0.0413	0.9272
CO	0.00312	0.9834	0.0546	0.9185
UHC	0.00205	0.9915	0.00423	0.9808
NOx	0.00193	0.9934	0.00375	0.9816
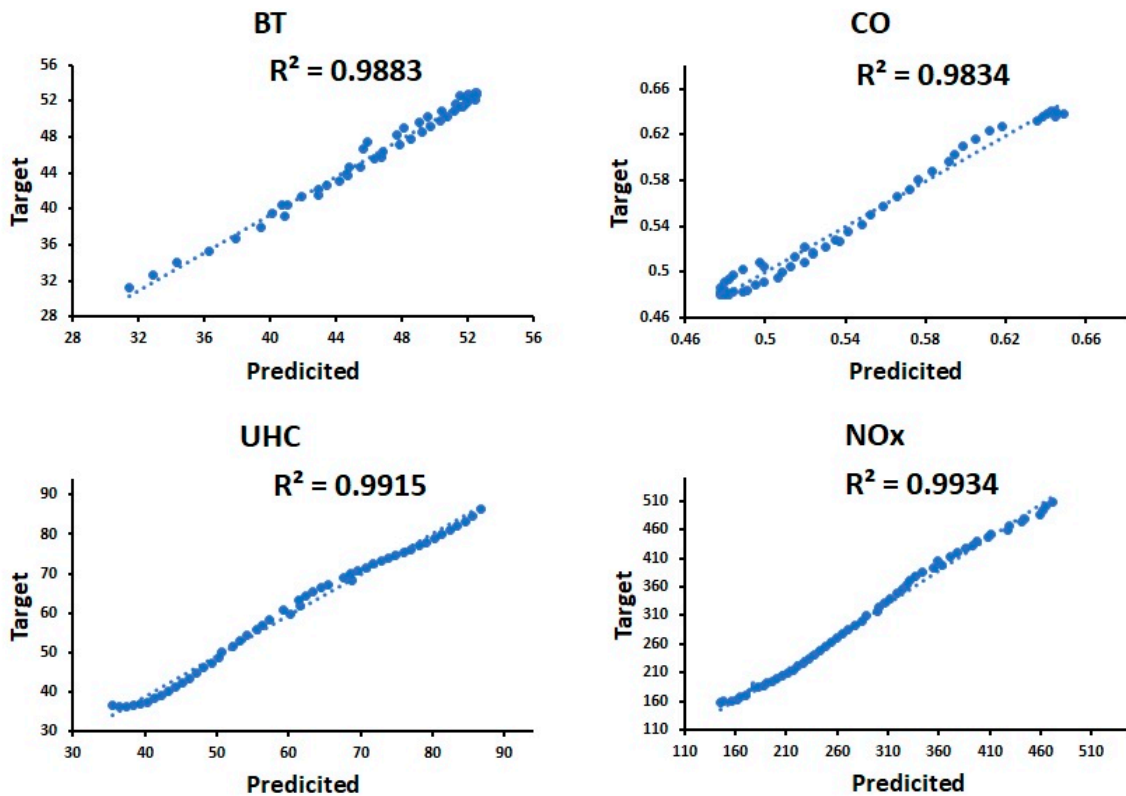
Figure 9. SVMR model prediction precision for each response.

3.3. Engine Performance and Emission Optimization

The optimization process is the next stage of our framework. The SHO method was used to optimize the output of the SVR model. The main target of the optimization process is to determine the optimal water addition and engine speed for different water percentages in the fuel mixture in order to decrease engine emissions (CO, UHC, and NOx) while optimizing engine performance (BT). Table 8 highlights the best outcomes for each response. According to the results, adding 5% water to the fuel mixture resulted in the highest BT (55.348 N.m) and lowest CO (0.479%) at engine speeds of 1877 and 1912 rpm, respectively. Regarding UHC and NOx, the lowest values were 35 and 112 ppm at engine speeds of 3000 and 1476 rpm, respectively, when 15% and 30% water were added to the fuel.

Table 8. Outcomes of the optimization process for each response in relation to the volume of water in the fuel mixture.

Experiment	Engine Speed (rpm)	Water%	Optimum Value
BT	1877	5%	55.348 N.m
CO	1912	5%	0.479%
UHC	3000	15%	35 ppm
NOx	1476	30%	112 ppm

Single-objective optimization is an efficient method for determining the best solution by maximizing or minimizing a single objective. Compared to single objective optimization, multiple objective optimizations can produce a set of non-dominated optimal solutions that help us understand the trade-offs between different goals [60]. In our framework, multi-objective optimization problems can be developed using weighting factors that combine different objectives into a single weighted objective. Table 9 lists the weights for each response that are used in the optimization process to determine the optimal value.

Table 9. The response weights that were employed in multi-objective optimization.

Response	Weight	Target
BT	0.3	Maximize
CO	0.2	Minimize
UHC	0.2	Minimize
NOx	0.3	Minimize

Table 10 shows the optimum engine speed and percentage of water added to reduce exhaust engine emissions while maximizing the engine performance. The added 15% water had better results in terms of engine emissions compared to pure diesel, which decreased by 5.2%, 22.938%, and 36.635% for CO, UHC, and NOx, respectively, at an engine speed of 1848 rpm. However, the engine performance in terms of BT was observed to decrease slightly by 5.973% when 15% water was added.

Table 10. Summary of multi-objective optimization results for all BT, CO, UHC, and NOx for various engine speeds and percentages of adding water to the fuel mixture.

Experiment	Engine Speed	Water%	BT	CO	UHC	NOx
Optimum values using SHO	1848	15%	49.503	0.5	57	369
Optimum values using WOA	1912	10%	52.252	0.48	62.3	404

The optimization of engine exhaust emissions and performance was achieved by comparing the performance of SHO with other meta-heuristic optimization techniques using the Whale Optimization Algorithm (WOA) as a reference. According to the findings in Table 10, SHO demonstrates a more robust potential for parallel optimization compared to WOA. This is attributed to SHO's advantages in terms of its ability to perform local exploitation effectively, achieve high precision in convergence, and its resilient design. The results highlight the investigation of Brownian motion throughout the world and the diverse offspring it produced. Furthermore, the adaptive parameter α and spiral motion in SHO play a role in guiding the optimization towards the ideal outcome, thus enhancing its accuracy in re-exploitation.

In conclusion, the results of this study were compared with previous research that utilized W/D emulsion fuels in CI engines, as shown in Table 11. The findings indicate that using W/D emulsion fuel has the potential to improve engine performance and decrease exhaust emissions from CI engines. However, prior studies did not always strike a balance between engine performance and emissions in determining the optimal water addition, which remains a major challenge in the automotive industry. It is acceptable to tolerate a small reduction in BT order to mitigate the environmental impact of diesel fuel.

Table 11. Compare the present study with other studies that utilized W/D emulsions in diesel engines.

Ref.	Diesel Engine Specification	Test Conditions	Water Content	Effect of the Engine Performance	Effect on the Exhaust Emission	Optimal Blend
Current Study	4 S, 4 C, DI, W–C	FL, VS (1000–3000) rpm	0–30% Vol., 5% increment Step	BT↑ until 5% water addition	EGT↓, CO_2↑ until 15%, CO↓ until 15%, UHC↑ until 15%, O_2↑, and NOx↓	15% (according SVR-SHO)
Ithnin et al., 2015 [20]	4 S, 1 C, A–C, 0.406 L	VL	0–20% Vol., 5% increment Step	BSFC↓	NOx↓, CO↑, PM↓, CO_2↓ @higher loads	20%
Hasannuddin et al., 2016 [61]	1 C, A–C, 400 CC	VL	0, 10, and 20% Vol.	FC↑	EGT↓, NOx↓, CO↑, PM↓, CO_2↓ and soot ↓	20%
El Shenawy et al., 2019 [62]	1 C, 825 CC	VL	0–9% Vol., 3% increment Step	BTE↑ and BSFC↓	NOx↓, CO↓, UHC↓, and smoke opacity ↓	9%
El-Din et al., 2019 [63]	1 C, A–C	VL	0, 5, 6, and 7% Vol.	BTE↑ and BSFC↓	NOx↓, CO↓, UHC↓, and smoke opacity ↓	7%
Jhalani et al., 2019 [64]	4 S, 1 C, DI, 661 CC, W–C	CS (1500 rpm), and VL	0–20% Vol., 5% increment Step	BTE↑	NOx↓, and smoke opacity ↓	15%
Hoseini and Sobati, 2019 [32]	4 stroke, Single cylinder, 510 CC	CS (1800 rpm), FL	0–20% Vol., 5% increment	PB↓, BT↓, BTE↑, and BSFC↑	CO↑, UHC↑, CO_2↑, and NOx↓	5%
Hassan et al., 2021 [65]	4 S, 1 C	VL	0–10% Vol., 2% increment step	BSFC↑ and BTE↓	CO↑, UHC↑, smoke↓, and NOx↓	10%
Alahmer et al., 2023 [59]	4 S, 4 C, DI, W–C	FL, VS (1000–3000) rpm	0–30% Vol., 5% increment Step	BP↑ until 5%, BSFC↓ until 10%, and BTE until 15%	NOx↓	9% (Applied of IGWO) 12% (Applied of GWO

S: Stroke, C: Cylinder, W–C: Water cooled; A–C: Air cooled VS: Variable engine speed, CS: Constant engine speed, FL: Full load, VL: Variable load, FC: Fuel consumption, EGT: Exhaust gas temperature; ↑: Increase; ↓: Decrease, GWO: grey wolf optimizer; and IGWO: intelligent grey wolf optimizer.

4. Conclusions

The SVR-SHO is proposed as a robust and innovative strategy for determining the optimal engine speed and water addition to W/D emulsion fuel for the operation of a four-cylinder diesel engine in this study. The CO, NOx, and UHC exhaust emissions were minimized, while the BT was maximized. The following are the most relevant findings from the experimental and optimization analyses:

- The W/D emulsion fuel combustion produced much less NOx than pure diesel. The decrease ranged from 3.22% to 67.14%, depending on the proportion of water added. This is due to the heat sink phenomenon, which lowers the adiabatic flame temperature.
- According to the experimental analysis, the highest reductions in UHC and CO were 15.63% and 9.57%, respectively, at 15% water addition compared to pure diesel. The reduction in UHC and CO emissions was due to the consequence of a micro-explosion process that might result in total combustion.
- The use of a nonlinear kernel (ANOVA radial basis) allows the SVR to model engine performance and emissions. The model performance was proven with an MSE of less than 0.0032 and an R^2 of more than 0.98.
- The SHO approach provides the optimum value with better exploration capability. The addition of 15% water to the W/D emulsion fuel reduced the engine emission levels as compared to pure diesel. It observed a decrease in CO, UHC, and NOx of 5.2%, 22.938%, and 36.635%, respectively, at an engine speed of 1848 rpm. However,

when 15% water was added, engine performance in terms of the BT was slightly reduced by 5.973%.

- The SVR model outperformed the ANN model, particularly for small datasets, because it was more robust to noisy data. Furthermore, local minima constitute a barrier for ANNs, implying that loss function minimization may fail.
- The SHO demonstrates a more robust potential for parallel optimization compared to WOA. This is attributed to SHO's advantages in terms of its ability to perform local exploitation effectively, achieve high precision in convergence, and its resilient design.

5. Future Works

The following areas will be thoroughly examined in future studies:

- The influence of the W/D emulsion fuel on fuel characteristics, such as a cetane number (CN), flash point (FP), and Fourier-transform infrared spectroscopy (FTIR).
- Examining the combustion characteristics of the fuel in a CI engine, including the combustion pressure profile, peak pressure rise rate, total heat release rate, ignition delay, combustion duration, and overall engine performance through energy and exergy assessments.
- Examining the impact of varying water droplet sizes on exhaust emissions, to determine the optimal droplet size for reducing pollutants.
- Analyzing the effect of different injection strategies, such as injection timing and pressure, on exhaust emissions.
- Investigating the long-term durability of the emulsion fuel and its impact on engine components such as injectors and fuel pumps.

Author Contributions: Conceptualization, A.A. and H.A.; methodology, H.A., A.A., M.I.A. and M.A.; software, H.A. and R.A.-R.; validation, A.A., R.A. and A.A.-M.; formal analysis, H.A., A.A. and R.A.; investigation, H.A., A.A. and M.A.; resources, A.A. and A.A.-M.; data curation, A.A.; writing—original draft preparation, H.A. and A.A.; writing—review and editing, H.A., A.A., M.I.A. and A.A.-M.; visualization, R.A.-R., R.A. and A.A.-M.; supervision, A.A.; project administration, A.A.; funding acquisition, A.A. All authors have read and agreed to the published version of the manuscript.

Nomenclature

List of Abbreviations

A–C	air cooled
ANN	artificial neural network
AI	artificial intelligent
BP	brake power
BSFC	brake-specific fuel consumption
BT	brake torque
BTE	brake thermal efficiency
C	cylinder
CI	compression ignition
CN	cetane number
CO	carbon monoxide
CO_2	carbon dioxide
CS	constant engine speed
DC	direct current

EGT	exhaust gas temperature
FC	fuel cell, fuel consumption
FL	full load
FP	flash point
FTIR	Fourier-transform infrared spectroscopy
GWO	grey wolf optimizer
IGWO	intelligent grey wolf optimizer
LB	lower bound
MSE	mean square error
ND-IR	nondispersive infrared
NOx	nitrogen oxides
PSO	particle swarm optimization
ReLU	rectified linear unit
RSM	response surface methodology
S	stroke
SHO	sea-horse optimizer
SVM	support vector machine
SO_2	sulfur dioxide
SVR	support vector regression
UHC	unburn hydrocarbon
UB	upper bound
VL	variable load
VS	variable engine speed
W–C	water cooled
W/D	water-in-diesel
WOA	whale optimization algorithm
WOT	wide-open throttle
List of symbols	
f(x)	function
$f(X_i)$	objective function
b	constant coefficient
C	penalty factor
s	seahorses
D	variable's dimension
R^2	coefficient of determination
P	population size
x, y, z	three-dimensional coordinates
x	n-dimensional input
rand	random number
i, j	integer
X_{best}	best individual
p	length of the stems
u, v	logarithmic spiral constants
$Levy(z)$	Lévy flight distribution function
l	constant coefficient
t	iteration
r_2, r_3	integer number
T	maximum number of iterations
X_i^{father}	male random
X_i^{mother}	female random
Greek symbols	
$\varphi(x)$	kernel function
ε	intense loss parameter
ξ_i, ξ_i^*	non-negative slack variables
ω	weight coefficient
α_i^*, α_i	Lagrangian multipliers
ω, k, λ	random positive number
β_t	Brownian motion random walk coefficient

References

1. Dębowski, M.; Michalski, R.; Zieliński, M.; Kazimierowicz, J. A Comparative Analysis of Emissions from a Compression–Ignition Engine Powered by Diesel, Rapeseed Biodiesel, and Biodiesel from Chlorella Protothecoides Biomass Cultured under Different Conditions. *Atmosphere* **2021**, *12*, 1099. [CrossRef]
2. Alahmer, A. Reduction a Particulate Matter of Diesel Emission by the Use of Several Oxygenated Diesel Blend Fuels. *Int. J. Therm. Environ. Eng.* **2014**, *7*, 45–50.
3. Gren, L.; Malmborg, V.B.; Jacobsen, N.R.; Shukla, P.C.; Bendtsen, K.M.; Eriksson, A.C.; Essig, Y.J.; Krais, A.M.; Loeschner, K.; Shamun, S. Effect of Renewable Fuels and Intake O2 Concentration on Diesel Engine Emission Characteristics and Reactive Oxygen Species (ROS) Formation. *Atmosphere* **2020**, *11*, 641. [CrossRef]
4. Zacharczuk, W.; Andruszkiewicz, A.; Tatarek, A.; Alahmer, A.; Alsaqoor, S. Effect of Ca-Based Additives on the Capture of SO2 during Combustion of Pulverized Lignite. *Energy* **2021**, *231*, 120988. [CrossRef]
5. Aladayleh, W.; Alahmer, A. Recovery of Exhaust Waste Heat for ICE Using the Beta Type Stirling Engine. *J. Energy* **2015**, *2015*, 495418. [CrossRef]
6. Alsaqoor, S.; Alahmer, A.; Aljabarin, N.; Gougazeh, M.; Czajczynska, D.; Krzyzynska, R. Effects of Utilization of Solid and Semi-Solid Organic Waste Using Pyrolysis Techniques. In Proceedings of the 2017 8th International Renewable Energy Congress (IREC), Amman, Jordan, 21–23 March 2017; pp. 1–5.
7. Gowrishankar, S.; Krishnasamy, A. Emulsification–A Promising Approach to Improve Performance and Reduce Exhaust Emissions of a Biodiesel Fuelled Light-Duty Diesel Engine. *Energy* **2023**, *263*, 125782. [CrossRef]
8. Adaileh, W.; Alahmer, A. Reduction of the Spark Ignition Engine Emissions Using Limestone Filter. *Can. J. Pure Appl. Scis* **2014**, *8*, 2761–2767.
9. Sridharan, G.; Chandramouli, R.; Musthafa, M.M.; Kumar, A.T. Performance, Combustion and Emission Characteristics of a Single Cylinder CI Engine Running on Diesel-Biodiesel-Water Emulsion with Additive. *Energy Sources Part A-Recovery Util. Environ. Eff.* **2019**. [CrossRef]
10. Yahaya Khan, M.; Abdul Karim, Z.A.; Hagos, F.Y.; Aziz, A.R.A.; Tan, I.M. Current Trends in Water-in-Diesel Emulsion as a Fuel. *Sci. World J.* **2014**, *2014*, 527472. [CrossRef]
11. Fahd, M.E.A.; Wenming, Y.; Lee, P.S.; Chou, S.K.; Yap, C.R. Experimental Investigation of the Performance and Emission Characteristics of Direct Injection Diesel Engine by Water Emulsion Diesel under Varying Engine Load Condition. *Appl. Energy* **2013**, *102*, 1042–1049. [CrossRef]
12. Alahmer, A. Influence of Using Emulsified Diesel Fuel on the Performance and Pollutants Emitted from Diesel Engine. *Energy Convers. Manag.* **2013**, *73*, 361–369. [CrossRef]
13. Yang, W.M.; An, H.; Chou, S.K.; Chua, K.J.; Mohan, B.; Sivasankaralingam, V.; Raman, V.; Maghbouli, A.; Li, J. Impact of Emulsion Fuel with Nano-Organic Additives on the Performance of Diesel Engine. *Appl. Energy* **2013**, *112*, 1206–1212. [CrossRef]
14. Liang, Y.; Shu, G.; Wei, H.; Zhang, W. Effect of Oxygen Enriched Combustion and Water–Diesel Emulsion on the Performance and Emissions of Turbocharged Diesel Engine. *Energy Convers. Manag.* **2013**, *73*, 69–77. [CrossRef]
15. Sudrajad, A.; Hirotsugu, F.; Ali, I. Experimental Study of Exhaust Emissions of W/O Emulsion Fuel in DI Single Cylinder Diesel Engine. *Mod. Appl. Sci.* **2011**, *5*, 73. [CrossRef]
16. Mazlan, N.A.; Yahya, W.J.; Ithnin, A.M.; Hasannuddin, A.K.; Ramlan, N.A.; Sugeng, D.A.; Adib, A.R.M.; Koga, T.; Mamat, R.; Sidik, N.A.C. Effects of Different Water Percentages in Non-Surfactant Emulsion Fuel on Performance and Exhaust Emissions of a Light-Duty Truck. *J. Clean. Prod.* **2018**, *179*, 559–566. [CrossRef]
17. Gonguntla, T.; Raine, R.; Ramsey, L.; Houlihan, T. Characteristics of Water-in-Diesel Emulsions in a Single Cylinder Compression Ignition Engine. In Proceedings of the ASME International Mechanical Engineering Congress and Exposition, American Society of Mechanical Engineers, Montreal, QC, Canada, 14–20 November 2014; Volume 46514, p. V06AT07A072.
18. Elsanusi, O.A.; Roy, M.M.; Sidhu, M.S. Experimental Investigation on a Diesel Engine Fueled by Diesel-Biodiesel Blends and Their Emulsions at Various Engine Operating Conditions. *Appl. Energy* **2017**, *203*, 582–593. [CrossRef]
19. Hasannuddin, A.K.; Yahya, W.J.; Sarah, S.; Ithnin, A.M.; Syahrullail, S.; Sugeng, D.A.; Razak, I.F.A.; Abd Fatah, A.Y.; Aqma, W.S.; Rahman, A.H.A. Performance, Emissions and Carbon Deposit Characteristics of Diesel Engine Operating on Emulsion Fuel. *Energy* **2018**, *142*, 496–506. [CrossRef]
20. Ithnin, A.M.; Ahmad, M.A.; Bakar, M.A.A.; Rajoo, S.; Yahya, W.J. Combustion Performance and Emission Analysis of Diesel Engine Fuelled with Water-in-Diesel Emulsion Fuel Made from Low-Grade Diesel Fuel. *Energy Convers. Manag.* **2015**, *90*, 375–382. [CrossRef]
21. Yang, W.M.; An, H.; Chou, S.K.; Vedharaji, S.; Vallinagam, R.; Balaji, M.; Mohammad, F.E.A.; Chua, K.J.E. Emulsion Fuel with Novel Nano-Organic Additives for Diesel Engine Application. *Fuel* **2013**, *104*, 726–731. [CrossRef]
22. Nour, M.; Abdel-Rahman, A.K.; Bady, M. Effect of Water Injection into Exhaust Manifold on Diesel Engine Combustion and Emissions. *Energy Procedia* **2016**, *100*, 178–187. [CrossRef]
23. Choi, I.; Lee, C. Numerical Study on Nitrogen Oxide and Black Carbon Reduction of Marine Diesel Engines Using Emulsified Marine Diesel Oil. *Sustainability* **2019**, *11*, 6347. [CrossRef]
24. Attia, A.M.A.; Kulchitskiy, A.R. Influence of the Structure of Water-in-Fuel Emulsion on Diesel Engine Performance. *Fuel* **2014**, *116*, 703–708. [CrossRef]

25. Lin, C.-Y.; Chen, L.-W. Engine Performance and Emission Characteristics of Three-Phase Diesel Emulsions Prepared by an Ultrasonic Emulsification Method. *Fuel* **2006**, *85*, 593–600. [CrossRef]

26. Alahmer, A.; Rezk, H.; Aladayleh, W.; Mostafa, A.O.; Abu-Zaid, M.; Alahmer, H.; Gomaa, M.R.; Alhussan, A.A.; Ghoniem, R.M. Modeling and Optimization of a Compression Ignition Engine Fueled with Biodiesel Blends for Performance Improvement. *Mathematics* **2022**, *10*, 420. [CrossRef]

27. Alahmer, A.; Ajib, S. Solar Cooling Technologies: State of Art and Perspectives. *Energy Convers. Manag.* **2020**, *214*, 112896. [CrossRef]

28. Alahmer, H.; Alahmer, A.; Alkhazaleh, R.; Alrbai, M. Exhaust Emission Reduction of a SI Engine Using Acetone–Gasoline Fuel Blends: Modeling, Prediction, and Whale Optimization Algorithm. *Energy Rep.* **2023**, *9*, 77–86. [CrossRef]

29. Alahmer, A.; Alahmer, H.; Handam, A.; Rezk, H. Environmental Assessment of a Diesel Engine Fueled with Various Biodiesel Blends: Polynomial Regression and Grey Wolf Optimization. *Sustainability* **2022**, *14*, 1367. [CrossRef]

30. Nassef, A.M.; Rezk, H.; Alahmer, A.; Abdelkareem, M.A. Maximization of CO_2 Capture Capacity Using Recent RUNge Kutta Optimizer and Fuzzy Model. *Atmosphere* **2023**, *14*, 295. [CrossRef]

31. Alahmer, A.; Alsaqoor, S. Simulation and Optimization of Multi-Split Variable Refrigerant Flow Systems. *Ain Shams Eng. J.* **2018**, *9*, 1705–1715. [CrossRef]

32. Hoseini, S.S.; Sobati, M.A. Performance and Emission Characteristics of a Diesel Engine Operating on Different Water in Diesel Emulsion Fuels: Optimization Using Response Surface Methodology (RSM). *Front. Energy* **2019**, *13*, 636–657. [CrossRef]

33. Vellaiyan, S.; Amirthagadeswaran, K.S.N. Multi-Response Optimization of Diesel Engine Operating Parameters Running with Water-in-Diesel Emulsion Fuel. *Therm. Sci.* **2017**, *21*, 427–439. [CrossRef]

34. Vellaiyan, S.; Subbiah, A.; Chockalingam, P. Multi-Response Optimization to Obtain Better Performance and Emission Level in a Diesel Engine Fueled with Water-Biodiesel Emulsion Fuel and Nanoadditive. *Environ. Sci. Pollut. Res.* **2019**, *26*, 4833–4841. [CrossRef] [PubMed]

35. Khathri, A.M.; Ismail, M.Y.; Abdullah, A.A.; Mamat, R. Performance, Exhaust Emissions and Optimization Using Response Surface Methodology of a Water in Diesel Emulsion on Diesel Engine. *J. Adv. Res. Fluid Mech. Therm. Sci.* **2022**, *93*, 1–12. [CrossRef]

36. Kumar, N.; Raheman, H.; Machavaram, R. Performance of a Diesel Engine with Water Emulsified Diesel Prepared with Optimized Process Parameters. *Int. J. Green Energy* **2019**, *16*, 687–701. [CrossRef]

37. Patil, H.; Gadhave, A.; Mane, S.; Waghmare, J. Analyzing the Stability of the Water-in-Diesel Fuel Emulsion. *J. Dispers. Sci. Technol.* **2015**, *36*, 1221–1227. [CrossRef]

38. Alahmer, A.I.; Adaileh, W.M.; Al Zubi, M.A. Monitoring of a Spark Ignition Engine Malfunctions Using Acoustic Signal Technique. *Int. J. Veh. Noise Vib.* **2014**, *10*, 201–213. [CrossRef]

39. Najafi, B.; Faizollahzadeh Ardabili, S.; Mosavi, A.; Shamshirband, S.; Rabczuk, T. An Intelligent Artificial Neural Network-Response Surface Methodology Method for Accessing the Optimum Biodiesel and Diesel Fuel Blending Conditions in a Diesel Engine from the Viewpoint of Exergy and Energy Analysis. *Energies* **2018**, *11*, 860. [CrossRef]

40. Vapnik, V.N. An Overview of Statistical Learning Theory. *IEEE Trans. Neural Netw.* **1999**, *10*, 988–999. [CrossRef]

41. Zhong, Z.; Carr, T.R. Application of Mixed Kernels Function (MKF) Based Support Vector Regression Model (SVR) for CO2–Reservoir Oil Minimum Miscibility Pressure Prediction. *Fuel* **2016**, *184*, 590–603. [CrossRef]

42. Zhang, F.; O'Donnell, L.J. Support Vector Regression. In *Machine Learning*; Elsevier: Amsterdam, The Netherlands, 2020; pp. 123–140.

43. Spall, J.C. *Introduction to Stochastic Search and Optimization: Estimation, Simulation, and Control*; John Wiley & Sons: Hoboken, NJ, USA, 2005; ISBN 0471441902.

44. Zhao, S.; Zhang, T.; Ma, S.; Wang, M. Sea-Horse Optimizer: A Novel Nature-Inspired Meta-Heuristic for Global Optimization Problems. *Appl. Intell.* **2022**, 1–28. [CrossRef]

45. Heywood, J.B. *Internal Combustion Engine Fundamentals*; McGraw-Hill Education: New York, NY, USA, 2018; ISBN 1260116107.

46. Alahmer, A.; Aladayleh, W. Effect Two Grades of Octane Numbers on the Performance, Exhaust and Acoustic Emissions of Spark Ignition Engine. *Fuel* **2016**, *180*, 80–89. [CrossRef]

47. Koc, A.B.; Abdullah, M. Performance and NOx Emissions of a Diesel Engine Fueled with Biodiesel-Diesel-Water Nanoemulsions. *Fuel Process. Technol.* **2013**, *109*, 70–77. [CrossRef]

48. Alahmer, A. Performance and Emission Assessments for Different Acetone Gasoline Blends Powered Spark Ignition Engine. *Int. J. Veh. Struct. Syst.* **2018**, *10*, 127–132. [CrossRef]

49. Lif, A.; Stark, M.; Nydén, M.; Holmberg, K. Fuel Emulsions and Microemulsions Based on Fischer–Tropsch Diesel. *Colloids Surf. A Physicochem. Eng. Asp.* **2010**, *354*, 91–98. [CrossRef]

50. Alahmer, A.; Yamin, J.; Sakhrieh, A.; Hamdan, M.A. Engine Performance Using Emulsified Diesel Fuel. *Energy Convers. Manag.* **2010**, *51*, 1708–1713. [CrossRef]

51. Jazair, W.; Kubo, S.; Takayasu, M.; Yatsufusa, T.; Kidoguchi, Y. Performance and Emission Characteristics of a Diesel Engine Fueled by Rapeseed Oil Bio-Fuel. *J. Mek.* **2011**, *33*, 2.

52. Farfaletti, A.; Astorga, C.; Martini, G.; Manfredi, U.; Mueller, A.; Rey, M.; De Santi, G.; Krasenbrink, A.; Larsen, B.R. Effect of Water/Fuel Emulsions and a Cerium-Based Combustion Improver Additive on HD and LD Diesel Exhaust Emissions. *Environ. Sci. Technol.* **2005**, *39*, 6792–6799. [CrossRef]

53. Sugeng, D.A.; Ithnin, A.M.; Yahya, W.J.; Kadir, H.A. Emulsifier-Free Water-in-Biodiesel Emulsion Fuel via Steam Emulsification: Its Physical Properties, Combustion Performance, and Exhaust Emission. *Energies* **2020**, *13*, 5406. [CrossRef]

54. De Giorgi, M.G.; Ciccarella, G.; Ficarella, A.; Fontanarosa, D.; Pescini, E. Effect of Jet-A1 Emulsified Fuel on Aero-Engine Performance and Emissions. In *AIP Conference Proceedings*; AIP Publishing LLC: Melville, NY, USA, 2019; Volume 2191, p. 20058.

55. Dryer, F.L. Water Addition to Practical Combustion Systems—Concepts and Applications. *Symp. Combust.* **1977**, *16*, 279–295. [CrossRef]

56. Ballester, J.M.; Fueyo, N.; Dopazo, C. Combustion Characteristics of Heavy Oil-Water Emulsions. *Fuel* **1996**, *75*, 695–705. [CrossRef]

57. Zeldvich, Y.B. The Oxidation of Nitrogen in Combustion and Explosions. *J. Acta Physicochim.* **1946**, *21*, 577.

58. Anetor, L.; Odetunde, C.; Osakue, E.E. Computational Analysis of the Extended Zeldovich Mechanism. *Arab. J. Sci. Eng.* **2014**, *39*, 8287–8305. [CrossRef]

59. Alahmer, H.; Alahmer, A.; Alkhazaleh, R.; Alrbai, M.; Alamayreh, M.I. Applied Intelligent Grey Wolf Optimizer (IGWO) to Improve the Performance of CI Engine Running on Emulsion Diesel Fuel Blends. *Fuels* **2023**, 35–57. [CrossRef]

60. Upcraft, T.; Guo, M. Phytoremediation Value Chains and Modeling. *Sustain. Remediat. Contam. Soil Groundw.* **2020**, 325–366. [CrossRef]

61. Hasannuddin, A.K.; Wira, J.Y.; Sarah, S.; Aqma, W.M.N.W.S.; Hadi, A.R.A.; Hirofumi, N.; Aizam, S.A.; Aiman, M.A.B.; Watanabe, S.; Ahmad, M.I. Performance, Emissions and Lubricant Oil Analysis of Diesel Engine Running on Emulsion Fuel. *Energy Convers. Manag.* **2016**, *117*, 548–557. [CrossRef]

62. El Shenawy, E.A.; Elkelawy, M.; Bastawissi, H.A.-E.; Shams, M.M.; Panchal, H.; Sadasivuni, K.; Thakar, N. Investigation and Performance Analysis of Water-Diesel Emulsion for Improvement of Performance and Emission Characteristics of Partially Premixed Charge Compression Ignition (PPCCI) Diesel Engines. *Sustain. Energy Technol. Assess.* **2019**, *36*, 100546. [CrossRef]

63. El-Din, M.R.N.; Mishrif, M.R.; Gad, M.S.; Keshawy, M. Performance and Exhaust Emissions of a Diesel Engine Using Diesel Nanoemulsions as Alternative Fuels. *Egypt. J. Pet.* **2019**, *28*, 197–204. [CrossRef]

64. Jhalani, A.; Sharma, D.; Soni, S.L.; Sharma, P.K. Effects of Process Parameters on Performance and Emissions of a Water-Emulsified Diesel-Fueled Compression Ignition Engine. *Energy Sources Part A Recover. Util. Environ. Eff.* **2019**, 1–13. [CrossRef]

65. Hassan, Z.U.; Usman, M.; Asim, M.; Kazim, A.H.; Farooq, M.; Umair, M.; Imtiaz, M.U.; Asim, S.S. Use of Diesel and Emulsified Diesel in CI Engine: A Comparative Analysis of Engine Characteristics. *Sci. Prog.* **2021**, *104*, 00368504211020930. [CrossRef]